A REAL-TIME WIDE-AREA CONTROL FOR MITIGATING SMALL-SIGNAL INSTABILITY IN LARGE ELECTRIC POWER SYSTEMS

By

JAIME QUINTERO RESTREPO

A dissertation submitted in partial fulfillment of
the requirements for the degree of

DOCTOR OF PHILOSOPHY

WASHINGTON STATE UNIVERSITY
School of Electrical Engineering and Computer Sciences

MAY 2005

To the Faculty of Washington State University:

The members of the Committee appointed to examine the dissertation of JAIME QUINTERO RESTREPO find it satisfactory and recommend that it be accepted.

_____

Chair

_____

_____

ACKNOWLEDGMENT

I would like to express my sincere gratitude to my advisor Professor Vaithianathan Venkatasubramanian for his guidance, enlightening instruction and support throughout my study at Washington State University.

I wish to thank Professor Anjan Bose and Professor Kevin Tomsovic for their instruction and valuable discussions on this work, and Professor Carl Hauser for his constructive and valuable interest. I also want to say thanks to all the other professors who have helped me during my studies here.

Specially, I want to remember Professor Chin Shung Hsu for his wonderful and friendly teaching.

Support from Power Systems Engineering Research Center (PSERC), Consortium for Electric Reliability Technology Solutions (CERTS), and Bonneville Power Administration (BPA) is gratefully acknowledged.

Also, I want to thank the support from Colciencias-Fulbright-Laspau program and the Universidad Autónoma de Occidente.

A REAL-TIME WIDE-AREA CONTROL FOR MITIGATING

SMALL-SIGNAL INSTABILITY IN LARGE

ELECTRIC POWER SYSTEMS

Abstract

by Jaime Quintero Restrepo, Ph.D.
Washington State University
May 2005

Chair: Mani V. Venkatasubramanian

This work proposes a real-time centralized controller for addressing small-signal instability related events in large electric power systems. The proposed system is meant to be a safety net type control strategy that will detect and mitigate small-signal stability phenomena as they emerge in the system. Specifically, it will use wide-area monitoring schemes to identify the emergence of growing or undamped oscillations related to interarea and/or local modes.

The damping levels of the associated interarea and local oscillatory modes will be estimated by analyzing predefined sets of signals using Multi-Prony method. Rules are developed for increasing Multi-Prony method's observability and dependability. These rules are applied to simulated signals, but also to real noisy measurements.

When the Central Control Unit detects an oscillatory interarea mode with low or negative damping ratio, say less than 1 percent, the controller will initiate strategically located Static VAR Compensator (SVC) devices, initially working in voltage regulation mode, into a full interarea active power damping operation for correcting the damping level of the problematic mode.

Rules for operating the SVC controls in the damping enhancement mode and for the application of the Multi-Prony algorithm on detecting the onset of the oscillations are proposed and tested in a two-area power system and in large scale simulation example.

The controller is shown to be effective on a validated western American large-scale power system model of the August 10, 1996 blackout event.

TABLE OF CONTENTS

LIST OF TABLES

LIST OF FIGURES

Dedication

To my mother Ana and father Oliver for giving me their best values.
To my brothers and sisters for their support.
To Paul y Libia for their unconditional support.
To Dr. Luis H. Perez, Enrique, Heberth, Henry and aunt Marina for believing in me.
To my wife Marcela, our children Jaime Eduardo and Pablo Alejandro for their courage and for giving me their true love.

CHAPTER ONE: INTRODUCTION

In modern day power systems, the power-flows across distant portions of the transmission network have been growing steadily to accommodate growing consumer demands. Moreover, owing to deregulation, the power transfers have also become somewhat unpredictable as dictated by market price fluctuations. As a result, the system operation can find itself close to or outside the secure operating limits under severe contingencies. Recent occurrences of large-scale blackouts all over the world reinforce the significance of developing safety net type control mechanisms, which are specifically designed to handle such unforeseen operating conditions [1], [2], [3].

Many efforts have been made in order to increase the damping of rotor modes under a wide range of operating conditions, allowing larger steady state power transmissions. Classical lead-lag and bang-bang compensators have been designed as auxiliary controls on Static VAR Compensators (SVC's) [4], [5], and [6]. Also, robust tuning algorithms has been used like the Linear Quadratic Gaussian (LQG) for SVC's in [7] and for Thyristor Controlled Series Capacitors (TCSC's) in [8], or $H\infty$ and μ-synthesis designs in [9] and [10] respectively. Since the interactions between uncoordinated damping controllers can be destabilizing, robust MIMO algorithms have also been developed for coordination of multiple Power System Stabilizers (PSS's) [11], [12], and [13], or multiple Flexible AC Transmission Systems (FACTS) [14], or various PSS units and FACTS together as in [15] and [16]. With the recent implementation of synchronized phasor measurements, wide-area measurement based coordinated control techniques have also been used [17]. Specific comparative studies may be found in [18] and [19].

Although, all of these techniques achieve very good results on improving the mode shape of the system and many achieve robust stability and robust performance over a

wide range of operating conditions, none of them is specifically designed for the emergency condition when the system may become small signal unstable. Therefore, the main purpose of this paper is to design a reliable emergency control strategy when the system despite all these well designed controls gets close to or goes into small signal instability.

The main difference in our approach from the previous research works is that the controller as proposed here will initiate targeted damping control actions *only* when it detects the emergence of small-signal instability in the power system. Therefore, this controller is aimed at being a *safety net type automatic supervisory mechanism* which is aimed towards handling growing or sustained oscillations from poor damping of interarea modes under unforeseen highly stressed operating conditions. It is meant to buy the system operators some time to react, by damping out the oscillations in the interim, while the operators can possibly initiate other corrective actions such as reducing the tie-line flows and/or initiate load shedding to relieve the system stress.

The controller is motivated towards preventing oscillatory instability events such as the August 10, 1996 western blackout that was caused by the negative damping of the 0.25 Hz western interarea mode (see Figure 1.1). Such oscillatory instability events typically take a minimum of four to five swings of growing oscillations before the oscillations become large enough to lead to system separation. Therefore, for such small-signal stability related instability events, there does exist sufficient time for an automatic controller such as the one postulated in Figure 1.2 to detect the event and to take corrective actions before the oscillations become critical.

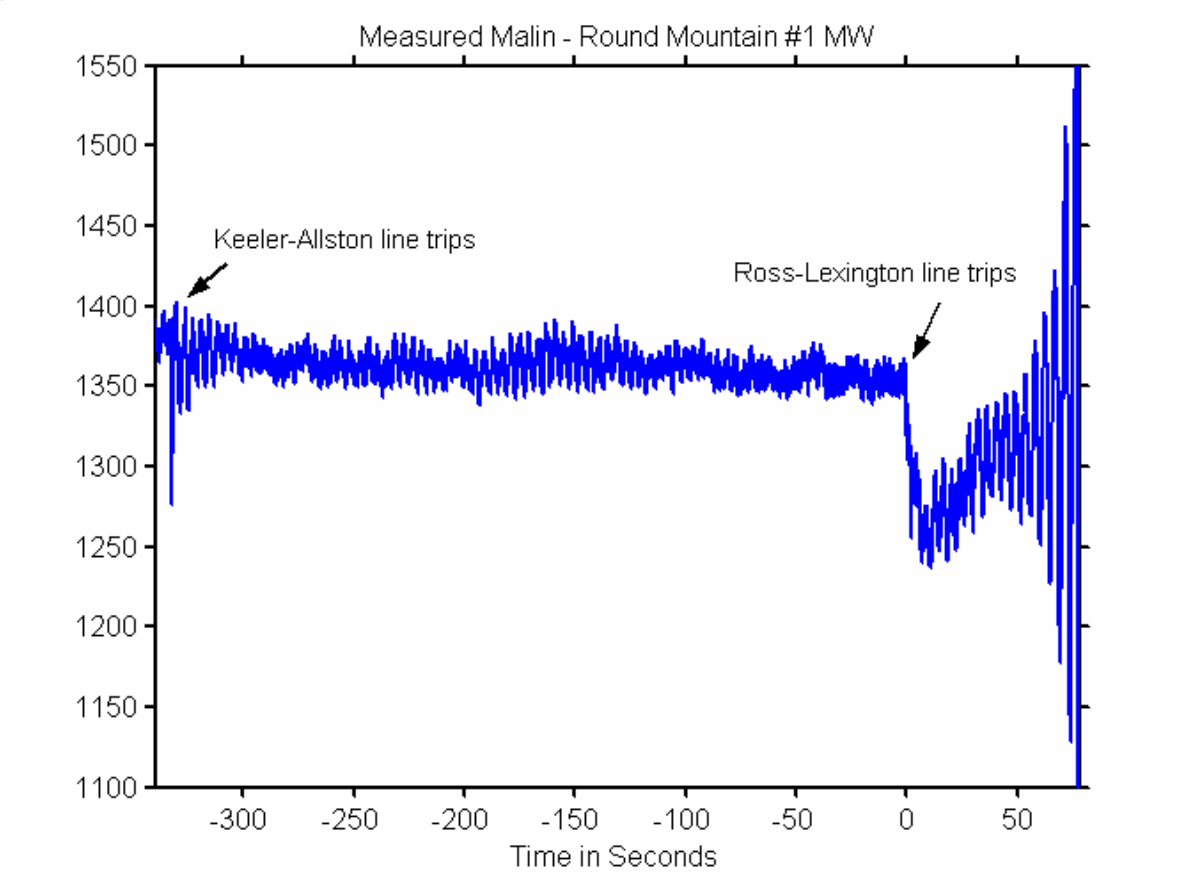

Figure 1.1: Growing oscillations on the California-Oregon tie lines during the August 10, 1996 blackout.

The controller framework is summarized in Figure 1.2. Rules for applying the right power swing phase compensation by strategically located Static VAR Compensators (SVC's) are developed. Also, they are demonstrated in the Kundur's two-area power system [20] and briefly in the Western Systems Coordinating Council (WSCC) large scale power system. Practical rules for applying multi-Prony analysis successfully on real-time basis for detection of low damped oscillations are developed. Offline rules for selection and use of the appropriate signals for improving the accuracy, the observability and reliability of multi-Prony analysis are obtained through simulations in the two-area

power system. Later, these rules are shown with real noisy data and final online rules are proposed and proved with the WSCC power system for a validated case of the August 10, 1996 blackout [21].

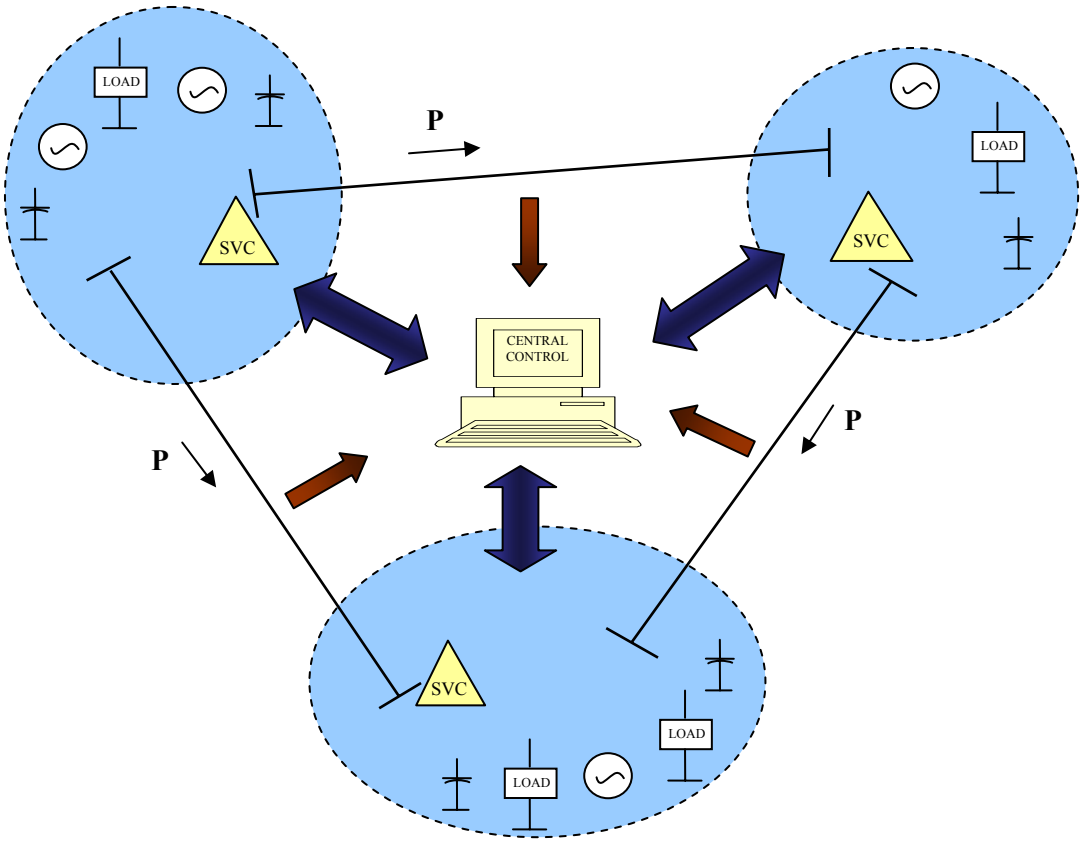

Figure 1.2: Real-Time Small-Signal-Stability Centralized Control Strategy

Prony analysis [22], has been successfully applied for offline signal and model identification in power systems [23], [24], [25], and a wide variety of fields [26], [27], [28]. It has been shown that comparing with Fourier transform based techniques, Prony's method is more powerful when it works [29]. Issues as system's nonlinearities [30], power system's high order model [31]and [32], noise, low signal to noise ratios (SNR)

and defining the time window or data length [33], [34] has limited its use in real-time applications.

In [30], an approach using the Hilbert transform to identify instantaneous attributes like amplitude, frequency and phase of nonlinear torsional shaft signals is presented. Even though this technique achieves good results, the absent of obtaining the modes damping ratio make it less suitable for real time small-signal stability assessment. On the other hand, [31] uses the single machine equivalent transient stability method to circumvent the problem of selecting some few signals to analyze a high complex real power system and [32] uses a reduced-order model in order to avoid the useless high frequency modes obtained by Prony. However, the problem suggested by [31] was already solved with one recent upgrade by [36], and the high frequency modes [32] are not an issue in small signal stability studies, since the low frequency nature of interarea and local modes. Reference [34] analyzes the issues of sample size selection, data length selection, and noise in Prony method. However, as seen later in this paper with simple rules and a smoothing filter these issues can be strongly reduced in Power System's small signal stability studies.

The proposed approach is based on previous works [35], [36], [37] and tested with real data and a validated simulation case [21]. Reference [35] introduces the applicability and usefulness of Prony in Power System, while [37] improves substantially the accuracy of Prony's estimations. Also, the idea of grouping signals by dominant modes to increase the observability of certain modes was first suggested in [36]. We have taken these previous results and developed some more rules to improve the accuracy, the reliability and the observability of the multi-Prony analysis for the purpose of a real-time controller.

Finally, the main objective of this work is on designing a practical real-time wide-area controller, independent of system configuration, to work as an automatic emergency

controller to improve dynamic security in the small signal sense. The main contributions are:

- Targets Small-Signal Instability.
- Improves Prony's Method Accuracy, Observability and Reliability.
- Analyzes the effects of full SVC PSDC location and compensation on interarea modes.
- Makes use of available resources.

Chapter Two describes the small-signal stability problem, and the mathematical concepts. The proposed control strategy, the assumptions, and the obtained benefits are explained briefly in Chapter Three. Through a practical example and a wide variety of computer simulations, Chapter Four shows how this centralized control strategy operates, and also compares with other available options. Our findings are tested in the WSCC system, in Chapter Five. Finally, some conclusions are given in Chapter Six.

CHAPTER TWO: THE SMALL-SIGNAL STABILITY PROBLEM

There are different kinds of stability problems in the Power System [21]. Here we deal with the problem of oscillatory instability when the system is subjected to small disturbances. Also, here stability is defined in the sense of Lyapunov [39]. The basic concepts that are needed to analyze the problem are shown next.

2.1 STABILITY IN THE SENSE OF LYAPUNOV

Consider the time-invariant system

$$\dot{\mathbf{x}} = \mathbf{f(x)}, \qquad \mathbf{x}(t_0) = \mathbf{x_0}. \tag{1}$$

Where, $\mathbf{x_0}$ is any equilibrium point. Then, the equilibrium point $\mathbf{x_0}$ is stable in the sense of Lyapunov if, for each $\varepsilon > 0$, there is a $\delta > 0$, $\delta \le \varepsilon$ such that

$$\|\mathbf{x}(t_0) - \mathbf{x}_0\| < \delta \Rightarrow \|\mathbf{x}(t) - \mathbf{x}_0\| < \varepsilon, \qquad \forall\, t \ge t_0$$

Suppose the local linearized approximation model of (1) is given by

$$\Delta \dot{\mathbf{x}} = \mathbf{A}\,\Delta \mathbf{x} \tag{2}$$

where, $\Delta \mathbf{x} = \mathbf{x} - \mathbf{x}_0$ and $\mathbf{A} = \left.\frac{\partial f}{\partial x}\right|_{\mathbf{x}_0}$. The equilibrium point $\mathbf{x_0}$ is locally asymptotically stable for (1) if all eigenvalues of the linearized Jacobian matrix **A** satisfy $\mathrm{Re}(\lambda_i) < 0$. On

the other hand, if **A** has one or more eigenvalues with positive real parts, the equilibrium point $\mathbf{x_0}$ is locally unstable for (1). If the eigenvalues of **A** satisfy only the weaker condition $\mathrm{Re}(\lambda_i) \leq 0$, local stability of $\mathbf{x_0}$ for (1) cannot be established using the linearized model (2) [39].

2.2 STATE SPACE REPRESENTATION OF POWER SYSTEMS

Mathematically, the Power System may be modeled by a set of nonlinear first order ordinary differential equations that represent the dynamic behavior of the system, and a set of algebraic equations that represent the power flows across the transmission network. Thus, the state space representation of a Power System maybe written as a differential-algebraic model

$$\begin{aligned} \dot{\mathbf{x}} &= \mathbf{f(x,w)} \\ \mathbf{0} &= \mathbf{g(x,w)}. \end{aligned} \tag{3}$$

For small disturbances, of interest is the behavior of the system around the nominal operating conditions $\mathbf{(x_0, w_0)}$. Consider $\mathbf{(x_0, w_0)}$ an equilibrium point such that

$$\begin{aligned} \mathbf{0} &= \mathbf{f(x_0, w_0)} \\ \mathbf{0} &= \mathbf{g(x_0, w_0)} \end{aligned} \tag{4}$$

Also, assume a small perturbation on the system and that the solution remains close to the nominal conditions, such that $\mathbf{x} = \mathbf{x_0} + \Delta\mathbf{x}$ and $\mathbf{w} = \mathbf{w_0} + \Delta\mathbf{w}$. From Taylor series and equations (3) and (4) we have that the linearized model is given by

$$\begin{aligned} \Delta\dot{\mathbf{x}} &= \mathbf{A}\,\Delta\mathbf{x} + \mathbf{B}\,\Delta\mathbf{w} \\ \mathbf{0} &= \mathbf{C}\,\Delta\mathbf{x} + \mathbf{D}\,\Delta\mathbf{w} \end{aligned} \tag{5}$$

where,

$$\mathbf{A} = \frac{\partial \mathbf{f}}{\partial \mathbf{x}}(\mathbf{x}_0, \mathbf{w}_0), \qquad \mathbf{B} = \frac{\partial \mathbf{f}}{\partial \mathbf{w}}(\mathbf{x}_0, \mathbf{w}_0),$$

$$\mathbf{C} = \frac{\partial \mathbf{g}}{\partial \mathbf{x}}(\mathbf{x}_0, \mathbf{w}_0), \qquad \mathbf{D} = \frac{\partial \mathbf{g}}{\partial \mathbf{w}}(\mathbf{x}_0, \mathbf{w}_0).$$

Assuming that the equilibrium point $(\mathbf{x}_0, \mathbf{w}_0)$ stays away from the singularity of the network equations, that is, when $\det\left(\frac{\partial \mathbf{g}}{\partial \mathbf{w}}(\mathbf{x}_0, \mathbf{w}_0)\right) \neq 0$, equation (5) can be written as

$$\Delta \dot{\mathbf{x}} = \mathbf{J}\, \Delta \mathbf{x} \tag{6}$$

where, $\mathbf{J} = \mathbf{A} - \mathbf{B}\mathbf{D}^{-1}\mathbf{C}$. Therefore, stability in the sense of Lyapunov may be established by the sufficient conditions on the eigenvalues of matrix **J**, [39].

An eigenvalue of the $n \times n$ square matrix **J** is defined as the real or complex number λ such that [40]

$$\mathbf{J}\mathbf{r} = \lambda \mathbf{r} \tag{7}$$

where, $\mathbf{r} \neq \mathbf{0}$. Any nonzero *n*-column vector **r** satisfying (7) is called a right eigenvector of **J** associated with λ. Similarly, an *n*-row vector **l** which satisfies

$$\mathbf{l}\mathbf{J} = \lambda \mathbf{l} \tag{8}$$

is called a left eigenvector of **J** associated with λ. There are *n* real or complex eigenvalues associated with **J**, they could be all distinct or not. Complex eigenvalues

occur in conjugate pairs. Without loss of generality, consider in this section having all distinct eigenvalues.

There are *n* right and *n* left independent eigenvectors associated to the *n* eigenvalues of **J**, and they can be normalized such that the right and left eigenvectors associated with the *i* eigenvalue are

$$\mathbf{l}_i \mathbf{r}_i = 1 \qquad \text{for} \quad i = 1,2,\ldots,n\,. \tag{9}$$

Therefore, the right and left modal matrices $\mathbf{R} = \begin{bmatrix} \mathbf{r}_1 & \mathbf{r}_2 & \ldots & \mathbf{r}_n \end{bmatrix}$ and $\mathbf{L} = \begin{bmatrix} \mathbf{l}_1{}^T & \mathbf{l}_2{}^T & \ldots & \mathbf{l}_n{}^T \end{bmatrix}^T$ are such that, $\mathbf{L} = \mathbf{R}^{-1}$.

As state in [41], the net associations between state variables and natural modes of matrix **J** may be taken from the participation matrix **P**. This matrix is obtained by an array multiplication of the right and left modal matrices, as

$$\mathbf{P} = \mathbf{R}.*\mathbf{L}^H \tag{10}$$

Here, the participation factor p_{ki} or *ki* element of matrix **P** gives the net participation of the *k*-state in the *i*-mode and vice versa.

Consider a system like (6), where $\mathbf{x}_0$ is any equilibrium state and $\mathrm{t}_0 = 0$. The solution in terms of eigenvalues λ_i, left eigenvectors $\mathbf{l_i}$, and right eigenvectors $\mathbf{r_i}$, may be written as

$$\Delta\mathbf{x}(\mathrm{t}) = \sum_{i=1}^{n} (\mathbf{l_i^T x_0}) \mathbf{r_i} \exp(\lambda_i \mathrm{t}) \qquad \textit{for} \quad \mathrm{t} \geq 0\,. \tag{11}$$

Since $\mathbf{l_i^T x_0}$ is a scalar and we may define $\mathbf{\Gamma_i} = \mathbf{r_i l_i^T}$ as a $n \times n$ residue matrix, we have that

$$\Delta\mathbf{x}(\mathrm{t}) = \sum_{i=1}^{n} \mathbf{\Gamma_i x_0} \exp(\lambda_i \mathrm{t}) \qquad \textit{for} \quad \mathrm{t} \geq 0\,. \tag{12}$$

Therefore, a single output of this system will be of the form

$$y(t) = \mathbf{c}\Delta\mathbf{x}(t) \qquad \textit{for} \quad t \geq 0\,. \tag{13}$$

CHAPTER THREE: THE PROPOSED CONTROLLER FRAMEWORK

The centralized control strategy introduced in this work (Figure 1.2) will constantly monitor the interarea modes, as well as the local modes presented in the power system. Data from predetermined signals with relevant content of local and interarea modes is sent from Phasor Measurement Units (PMU's) at different control areas and intertie lines to the central control unit via suitable communication channels. The central controller analyzes these signals in the form of different sets by using Multi-Prony's method grouped by dominant modes, in order to estimate the power system's mode shape. If there is one or more under damped interarea modes, the central unit will issue triggers to previously identified SVC's located at the affected areas and or along the intertie lines. The SVC's will switch from the voltage regulation control mode to the full Power Swing Damping Control (PSDC) mode until safe damping ratio values ζ_i and safe operating conditions are reached again. Constant monitoring will assure that other local nor interarea modes are not weakened during the control action.

The controller framework may be viewed as follows:

A. *The Central Control Unit*

A series of offline rules based on Prony analysis and wide-area measurements are designed for ensuring the observability and redundancy of the multi-Prony oscillation detection algorithm. Also, online rules are derived for increased reliability.

Offline Rules

Selecting and using the appropriate signals.

1) Defining the data length (or the period of the time window) for the Prony analysis.
2) Grouping signals by dominant modes for ensuring redundancy and for cross-checking the results of Multi-Prony modal estimation.
3) Grouping signals by using mode contents for monitoring all the typical interarea modes in the Prony analysis.
4) Verifying the Prony oscillation detection methodology by off-line transient stability type simulations and recent event recordings.

Online Rules

1) Algorithm specifics for when the oscillations are considered critical enough to activate the emergency controller
2) Multi-Prony estimation rules for ensuring reliability through crosschecking of estimation results from different groups and from overlapping time intervals.
3) Selecting an appropriate SVC by combining the offline rules together with online monitoring of the SVC responses during the current event.
4) Determining the type of PSDC control at the SVC from the active power flow direction of the interarea active power-flow (Section V) that is used as the input for SVC PSDC control design.

B. ***The SVC local unit***

The selected SVC is triggered from Voltage Regulation form to full PSDC operation by the Central Unit. Also, the central control unit provides the remote input for the SVC PSDC control in the form of the critical intertie active power flow. The central control unit also suggests the type of PSDC design to the SVC by using the following simple rule:

1) SVC PSDC is designed as a phase lag compensator if the SVC is at the sending side for the active power-flow of the intertie line that is being used as the control input.
2) SVC PSDC is designed as a phase lead compensator if the SVC is at the receiving side for the active power-flow of the intertie line that is being used as the control input.

With the existing technology of wide-area measurements, fiber optic communications, fast computers, and Prony's algorithm this controller will be able to detect an under damped or negative damped interarea oscillation. The controller can then initiate the appropriate control actions in a very short time frame, often in only three or four swings. This makes this automatic controller suitable to address the small-signal instability problem in a real-time operating environment. A more detailed explanation of each component is presented next.

3.1 THE CENTRAL CONTROL UNIT

Selected signal measurements, received from dedicated Phasor Measurement Units (PMU), grouped by dominant modes are processed by the central control unit using Multi-Prony analysis [37].

The data suitable for Prony analysis, is the one collected after a small or medium-scale disturbance. The initial period of fast and very nonlinear oscillations just after the disturbance will give bad estimations, since Prony's method is a linear approach. We present techniques for distinguishing between useful versus unreliable Prony estimations of modal data, from real-time measurement data. Also, we show that two or three swings of data are sufficient to obtain a fair approximation of the mode shape. These concepts are presented through detailed examples in Chapters Four and Five.

It has been demonstrated in [37] that Multi-Prony analysis of various signals is more robust than single Prony analysis. Also, it was noted in [36] that the Prony accuracy is improved by having different signals with the same dominant mode analyzed simultaneously. Moreover, our tests have shown that the observability on the estimation of interarea and local modes is increased by analyzing different sets of signals grouped by dominant modes. In extension, for the common case of having two or more interarea or local area modes with almost the same frequency, it is likely that the Prony's method will have difficulties on differentiating these modes if we try to extract the information from a single signal or a single set of signals, as shown next. We have addressed this problem by analyzing the signals in different sets, previously characterized by dominant modes. That is, the signals with the same dominant mode are grouped together, and we form a few such different sets to ensure redundancy.

Moreover, it is not unusual in Prony's analysis to make bad estimations from a signal set at any time. Crosschecking results from different sets of data will make sure that our estimations are reliable and will provide a certain redundancy level. In case of bad estimations, the analysis will be repeated over those sets using another least square solution. If the results are still not consistent, the total estimations would be disregarded, and a complete new estimation process should be applied over the next time window.

Based on the estimated mode (eigenvalue) parameters, if the central controller determines that one or more interarea modes are under damped or negative damped, it will send triggers to corresponding SVC's.

3.1.1 Signal Modeling with Prony's Method

Prony's method, or Multi-Prony's method, estimates parameters of modes associated with a signal, or certain set of signals. These are mode frequency f_i, amplitude A_i, phase ϕ_i, and damping ratio ζ_i. The Prony's method which was originated in a very early

century [22], [35], calculates (12) or (13) estimations by approximating in the least square sense to a certain set of equally sampled discrete data, a linear exponential function of the form

$$\hat{y}(t) = \sum_{i=1}^{m} A_i \exp(\sigma_i t)\cos(2\pi f_i t + \phi_i) \qquad for \quad t \geq 0 \tag{14}$$

The real equation (14) may be written in a complex exponential form as

$$\hat{y}(t) = \sum_{i=1}^{m} B_i \exp(\lambda_i t) + B_i^* \exp(\lambda_i^* t) \qquad for \quad t \geq 0 \tag{15}$$

where, m is the number of modes, $B_i = \frac{A_i}{2}\exp(j\phi_i)$, $\lambda_i = \sigma_i + j\omega_i$, and * indicates complex conjugate. Moreover, in a simplified manner (15) could be expressed as

$$\hat{y}(t) = \sum_{i=1}^{p} B_i \exp(\lambda_i t) \qquad for \quad t \geq 0\,. \tag{16}$$

where, p is the number of the estimated eigenvalues.

Consider also that, for equations (15) or (16) the B_i's and the λ_i's are distinct.

Let $y(t)$ be N samples evenly spaced by Δt such that,

$$y(t_k) = y(k) \qquad for \quad k = 0,1,\ldots,N-1\,.$$

The Prony's estimated output signal at time $t_k = k$ will be

$$\hat{y}(k) = \sum_{i=1}^{p} B_i \exp(\lambda_i \, k \, \Delta t) \qquad for \quad k = 0,1,\ldots,N-1 .$$

For convenience, define $z_i = \exp(\lambda_i \Delta t)$, then

$$\hat{y}(k) = \sum_{i=1}^{p} B_i z_i^k \qquad for \quad k = 0,1,\ldots,N-1 . \tag{17}$$

As can be seen, the objective with Prony's method is to find the values of B_i and z_i that produce

$$\hat{y}(k) = y(k) \qquad for \quad all \quad k \tag{18}$$

Assuming that equation (18) is true for all k, set

$$\begin{aligned}
y(0) &= B_1 + B_2 + \cdots + B_p \\
y(1) &= B_1 z_1 + B_2 z_2 + \cdots + B_p z_p \\
y(2) &= B_1 z_1^2 + B_2 z_2^2 + \cdots + B_p z_p^2 \\
&\vdots \qquad\qquad \vdots \\
y(N-1) &= B_1 z_1^{N-1} + B_2 z_2^{N-1} + \cdots + B_p z_p^{N-1}
\end{aligned} \tag{19}$$

In matrix form,

$$\begin{bmatrix} y(0) \\ y(1) \\ y(2) \\ \vdots \\ y(N-1) \end{bmatrix} = \begin{bmatrix} z_1^0 & z_2^0 & \cdots & z_p^0 \\ z_1^1 & z_2^1 & \cdots & z_p^1 \\ z_1^2 & z_2^2 & \cdots & z_p^2 \\ & \vdots & \vdots & \\ z_1^{N-1} & z_2^{N-1} & \cdots & z_p^{N-1} \end{bmatrix} \begin{bmatrix} B_1 \\ B_2 \\ \vdots \\ B_p \end{bmatrix} \tag{20}$$

Note that these equations are nonlinear in z and that we need $N \geq 2p+1$.

The method to solve the above equations may be described as follows: Let z_i for $i = 1,2,\ldots, p$ be the roots of some *p*th order polynomial $\pi(z)$ [42]:

$$\pi(z) = (z - z_1)(z - z_2)\ldots(z - z_p) = z^p - \alpha_1 z^{p-1} - \ldots - \alpha_{p-1} z - \alpha_p = 0 \qquad (21)$$

Now, multiply the first equation in (19) by $-\alpha_p$, the second equation by $-\alpha_{p-1}$, …, the *p*th equation by $-\alpha_1$, and the *(p+1)*th equation by 1, and add the results. Then,

$$\mathrm{y}(p) - \alpha_1\,\mathrm{y}(p-1) - \alpha_2\,\mathrm{y}(p-2) - \ldots - \alpha_p\,\mathrm{y}(0) =$$
$$B_1(z_1^p - \alpha_1 z_1^{p-1} - \alpha_2 z_1^{p-2} - \ldots - \alpha_p z_1^0) + B_2(z_2^p - \alpha_1 z_2^{p-1} - \alpha_2 z_2^{p-2} - \ldots - \alpha_p z_2^0) + \ldots$$

Since equation (21) is true for all z_i, the right-hand members of the above equation vanish and it is obtained that

$$\mathrm{y}(p) = \alpha_1\,\mathrm{y}(p-1) + \alpha_2\,\mathrm{y}(p-2) + \ldots + \alpha_p\,\mathrm{y}(0) \qquad (22)$$

Applying repeatedly the above process starting this time from the second equation in (19), and next from the third equation, and so on, the following $N - 1 - p$ set of linear equations can be obtained

$$\begin{bmatrix} \mathrm{y}(p) \\ \mathrm{y}(p+1) \\ \mathrm{y}(p+2) \\ \vdots \\ \mathrm{y}(N-1) \end{bmatrix} = \begin{bmatrix} \mathrm{y}(p-1) & \mathrm{y}(p-2) & \cdots & \mathrm{y}(0) \\ \mathrm{y}(p) & \mathrm{y}(p-1) & \cdots & \mathrm{y}(1) \\ \mathrm{y}(p+1) & \mathrm{y}(p) & \cdots & \mathrm{y}(2) \\ & \vdots & \vdots & \\ \mathrm{y}(N-2) & \mathrm{y}(N-3) & \cdots & \mathrm{y}(N-p-1) \end{bmatrix} \begin{bmatrix} \alpha_1 \\ \alpha_2 \\ \vdots \\ \alpha_p \end{bmatrix} \qquad (23)$$

This set of equations can be solved directly if $N = 2p + 1$, or approximately by least squares if $N > 2p + 1$. There are very well known solutions to the least square problem

[43]. The Toolbox [36] developed by BPA/PNNL that we used for our next application example has three solution approaches: The Singular Value Decomposition (SVD) method, the QR decomposition, and the Total Least Square (TLS) solution.

Once the α's are obtained, the z_i's values could be found from equation (21). Then, equations (20) become linear with known coefficients and the B_i's may be determined. Note that B_i's have the information about amplitude and initial phase of the modes, while the z_i's content the values for σ_i and ω_i of the modes.

Multi-Prony analysis [37] is a vector-matrix extension of Prony analysis, considering multiple outputs at the same time.

3.2 THE LOCAL SVC UNIT

This control strategy assumes that some of the SVC units have been earmarked for potential operation under the proposed scheme, and that these SVC's are normally operating in the voltage regulation mode. Specifically, when the SVC receives the external trigger from the central control unit, the SVC will switch to full PSDC form.

The SVC mode switch occurs only when the oscillations are already so large as to threaten the integrity of the large system. Under such highly stressed conditions, we assume that the SVC's can be switched to the full damping control mode to quickly damp out the otherwise growing (or sustained) oscillations in the system. The damping control at the SVC's will be designed by using the active power flow from a specific intertie line as the control input signal. The details will be discussed in Chapters Four and Five.

As shown in section 4.2**,** the use of a full PSDC operation gives a more effective way of damping interarea oscillations compared with the supplementary control action shown in [21]. As we will demonstrate in section 4.2.1, the damping control actions of an SVC

working on full PSDC located at the sending or at the receiving sides of an intertie line are more effective than those of an SVC located close to the middle of the intertie line. Additionally, as seen in our results, an SVC located at the active power sending area offers the most effective location for full PSDC when the respective inter-tie active power flow is used as the control input for the SVC damping control.

If the SVC is located at the *active power sending side*, the PSDC output signal of the SVC should be designed to be *lagging* the interarea active power flow signal. While, if the SVC is *at the receiving side,* the PSDC output should be designed to *lead* the interarea active power flow. The necessary formulation is presented next.

When an SVC is located close to a critical inter-tie line, it is easy to determine whether the SVC is at the sending or receiving end of the tie line by monitoring the active power-flow on the line. Therefore, the design of the SVC damping control logic becomes very simple for real-time implementation, and is specifically suited for stressed operating conditions when the topology or the underlying model of the power system may be uncertain. Based on the active power-flow direction of the intertie line, whose MW power-flow signal is used as the SVC control input, the SVC damping control is designed to lag or lead the MW input, depending on whether the SVC is at the sending or receiving end of the active power-flow on the tie line respectively.

The distinction of whether the SVC is at the sending or receiving end is far more complicated, when an SVC is located far from the two ends of the inter-tie line in a meshed power system. For these cases, the angle admittance sensitivity factors described in Chapter Four may be used, and the discussion is deferred to a next future. In this work, we assume that the SVC to be used for the damping control purposes can be clearly identified as being at the sending or receiving end of the critical inter-tie line which contributes the active power-flow control input signal for the SVC.

3.2.1 The Classical Power System Model

In this work, we are interested on making an analytic study of the effects of the SVC location with respect to an intertie line, on the associated interarea mode. In order to keep a low order model for our analysis purposes, generators are modeled for this part using a classical representation or swing equation (24), which includes only two state variables per generator, rotor angle δ and rotor speed deviation $\Delta\omega$. Since interarea modes are mainly associated with these two state generator variables, interarea modes are still presented and their characteristics are preserved when using this simple classical model for analytical study. Later, in next chapters, we show that the design rules that are derived from the classical model appear to be valid in simulations of detailed models as well as for a large power system model.

The swing equation for a generator may be written as [21],

$$\dot{\delta} = \Delta\omega$$

$$\Delta\dot{\omega} = \frac{\omega_s}{2H}\left[P_m - P_e - K_D\left(\frac{\Delta\omega}{\omega_s}\right)\right] \tag{24}$$

where $\Delta\omega = \omega - \omega_s$ and ω_s is the synchronous speed, P_m is the shaft mechanical power in pu, P_e is the air-gap power in pu, and K_D is a damping factor that includes mechanical and electrical damping components.

Briefly, the classical representation can be derived from detailed power system models by making the following assumptions [44]:

- Mechanical power is constant.
- Damping and synchronizing torques can be approximated.

- The voltage magnitude E, behind the transient reactance machine model, is constant.
- The machine rotor angle δ coincides with the angle of the voltage behind the transient reactance.
- Loads are of the constant impedance type.

Moreover, with generators characterized by the transient reactance machine model and loads by constant impedances, the interconnected transmission network represented by

$$\mathbf{I} = \mathbf{YV} \tag{25}$$

may be partitioned as

$$\begin{bmatrix} \mathbf{I}_G \\ \mathbf{0} \end{bmatrix} = \begin{bmatrix} \mathbf{Y}_{GG} & \mathbf{Y}_{GR} \\ \mathbf{Y}_{RG} & \mathbf{Y}_{RR} \end{bmatrix} \begin{bmatrix} \mathbf{V}_G \\ \mathbf{V}_R \end{bmatrix} \tag{26}$$

where, subscript G relates to all internal generators nodes and subscript R comprises the remaining nodes with zero injection current. Reducing equation (26) by eliminating $\mathbf{V}_R$, we obtain

$$\mathbf{I}_G = \left(\mathbf{Y}_{GG} - \mathbf{Y}_{GR}\mathbf{Y}_{RR}^{-1}\mathbf{Y}_{RG}\right)\mathbf{V}_G . \tag{27}$$

Defining $\mathbf{Y}_{GEN}$ as,

$$\mathbf{Y}_{GEN} = \mathbf{Y}_{GG} - \mathbf{Y}_{GR}\mathbf{Y}_{RR}^{-1}\mathbf{Y}_{RG} \tag{28}$$

we may write

$$\mathbf{I}_G = \mathbf{Y}_{GEN}\mathbf{V}_G \tag{29}$$

or,

$$\vec{\mathrm{I}}_{Gi} = \sum_{j=1}^{ng} \vec{\mathrm{Y}}_{GENij}\vec{\mathrm{V}}_{Gj} \qquad for \quad i = 1,\ldots,ng \tag{30}$$

where *ng* is the number of generators.

From (30) and considering that air-gap power P_e is equal to generator active output power *P*, neglecting stator resistance we may write that

$$P_i = \sum_{j=1}^{ng} E_{Gi}E_{Gj}Y_{GENij}\cos(\delta_i - \delta_j - \varphi_{GENij}) \quad for\ i = 1,\ldots,ng\,. \tag{31}$$

Initial values may be found from a pre-transient power flow load study.

3.2.2 The Linearized State Space Classical Model for a Reduced Two-Area Power System

The Two-Area Power System presented by Kundur [20] will be used in this work, Figure 3.1. Although this is a small test system, the system has been proven to be of great value for the study of interarea oscillations in real power systems. Here, we also reduce the original power system of four generators as present in Figure 3.1, to only two generators.

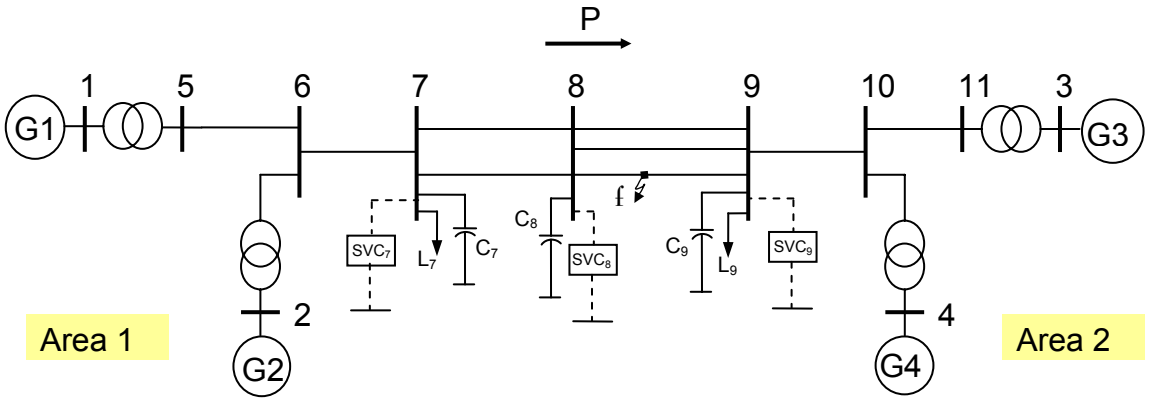

Figure 3.1: Two-area Power System

The compensator model used for the SVC in full Power Swing Damping Control (PSDC) operating mode, in this modeling case, is given only for a Low Pass Filter followed by a Phase Compensation Filter. Then, the PSDC model equations are

$$\begin{aligned} \dot{e}_{LP} &= \frac{1}{T_{2LP}}\left(P_{79REF} - P_{79} - e_{LP}\right) \\ \dot{B}_{SVC} &= \frac{1}{T_2}\left[K\left(e_{LP} + T_1\dot{e}_{LP}\right) - B_{SVC}\right] \end{aligned} \tag{32}$$

where, P_{79} is the interarea active power flow

$$P_{79} = \frac{V_7 V_9}{X_{79}}\sin(\theta_7 - \theta_9)\,, \tag{33}$$

$\vec{\mathrm{V}}_7, \vec{\mathrm{V}}_9$ bus voltages may be obtained approximately by

$$\begin{aligned} \vec{\mathrm{V}}_7 &\cong E_1\angle\delta_1\left[1 - \left(\vec{\mathrm{Y}}_{GEN11} + \vec{\mathrm{Y}}_{GEN12}\right)\left(jX'_{d1} + jX_{T1} + jX_{56} + jX_{67}\right)\right] \\ \vec{\mathrm{V}}_9 &\cong E_2\angle\delta_2\left[1 - \left(\vec{\mathrm{Y}}_{GEN22} + \vec{\mathrm{Y}}_{GEN21}\right)\left(jX'_{d2} + jX_{T2} + jX_{11-10} + jX_{10-9}\right)\right]. \end{aligned} \tag{34}$$

The nonlinear state space model (3) for the Two-area power system of Figure 3.1 is defined by equations (24), (28), (31), (32), (33), and (34). The state space variables are $\mathbf{x} = \begin{bmatrix} \delta_1 & \Delta\omega_1 & \delta_2 & \Delta\omega_2 & e_{LP} & B_{SVC} \end{bmatrix}^T$. An equilibrium point for the generated nonlinear state space model can be calculated by

$$
\begin{aligned}
\delta_{1_0} &= \cos^{-1}\left[\frac{P_{m1} - Y_{GEN11_0} E_1^2 \cos(\varphi_{GEN11_0})}{Y_{GEN12_0} E_1 E_2}\right] + \delta_{2_0} + \varphi_{GEN12_0} \\
\Delta\omega_{1_0} &= 0 \\
\delta_{2_0} &= \cos^{-1}\left[\frac{P_{m2} - Y_{GEN22_0} E_2^2 \cos(\varphi_{GEN22_0})}{Y_{GEN21_0} E_2 E_1}\right] + \delta_{1_0} + \varphi_{GEN21_0} \\
\Delta\omega_{2_0} &= 0 \\
e_{LP_0} &= P_{79REF} - \left[\frac{V_{7_0} V_{9_0}}{X_{79}} \sin(\theta_{7_0} - \theta_{9_0})\right] \\
B_{SVC_0} &= K e_{LP_0}.
\end{aligned}
\tag{35}
$$

Therefore, the Jacobian matrix **J** in (6) around the equilibrium point (35) for this Two-area power system, may be written as

$$
\mathbf{J} = \begin{bmatrix}
0 & 1 & 0 & 0 & 0 & 0 \\
J_{21} & -\dfrac{K_{D1}}{2H_1} & J_{23} & 0 & 0 & a \\
0 & 0 & 0 & 1 & 0 & 0 \\
J_{41} & 0 & J_{43} & -\dfrac{K_{D2}}{2H_2} & 0 & b \\
J_{51} & 0 & J_{53} & 0 & -\dfrac{1}{T_{2LP}} & c \\
J_{61} & 0 & J_{63} & 0 & d & e
\end{bmatrix}.
\tag{36}
$$

where the following **J** parameters depend mostly on the initial values and the power system configuration. If we neglect the variations in voltage magnitudes, these are constant for the different PSDC phase compensators tested:

$$J_{21} = \frac{\omega_s Y_{GEN12_0} E_1 E_2}{2H_1} \sin\left(\delta_{1_0} - \delta_{2_0} - \varphi_{GEN12_0}\right)$$
$$J_{23} = -J_{21} \tag{37}$$
$$J_{41} = -\frac{\omega_s Y_{GEN21_0} E_1 E_2}{2H_2} \sin\left(\delta_{2_0} - \delta_{1_0} - \varphi_{GEN21_0}\right)$$
$$J_{43} = -J_{41}.$$

The next **J** values are affected by the low pass filter design included in the PSDC function, and are independent of the other PSDC variables:

$$J_{51} = -\frac{1}{T_{2LP} X_{79}} \left[\frac{\partial V_7}{\partial \delta_1} V_{9_0} \sin\left(\theta_{7_0} - \theta_{9_0}\right) + \frac{\partial \theta_7}{\partial \delta_1} V_{7_0} V_{9_0} \cos\left(\theta_{7_0} - \theta_{9_0}\right) \right]$$
$$J_{53} = -\frac{1}{T_{2LP} X_{79}} \left[\frac{\partial V_9}{\partial \delta_2} V_{7_0} \sin\left(\theta_{7_0} - \theta_{9_0}\right) - \frac{\partial \theta_9}{\partial \delta_2} V_{7_0} V_{9_0} \cos\left(\theta_{7_0} - \theta_{9_0}\right) \right]. \tag{38}$$

For convenience in analysis, we set the gain K as $K = T_2/T_1$ so that the compensator transfer function is of the pole-zero form $G_c(s) = \frac{s + 1/T_1}{s + 1/T_2}$. We study the impact of the phase-lead and phase-lag provided by the compensator on the damping of the interarea mode, since they were the dominant contributors to the overall effectiveness of the compensator. The compensator gain has a lesser impact on the damping as compared

with the phase, as we have been able to test through our simulations. With the gain K, $K = T_2/T_1$, the parameters satisfy the following property

$$J_{61} = \frac{KT_1}{T_2} J_{51} = J_{51}$$

$$J_{63} = \frac{KT_1}{T_2} J_{53} = J_{53}. \tag{39}$$

On the other hand, the following parameters are going to change according to the SVC location

$$\begin{aligned} a = \frac{\omega_s}{2H_1}[& -\frac{\partial Y_{GEN11}}{\partial B_{svc}} E_1^2 \cos\left(\varphi_{GEN11_0}\right) \\ & + \frac{\partial \varphi_{GEN11}}{\partial B_{svc}} Y_{GEN11_0} E_1^2 \sin\left(\varphi_{GEN11_0}\right) \\ & - \frac{\partial Y_{GEN12}}{\partial B_{svc}} E_1 E_2 \cos\left(\delta_{1_0} - \delta_{2_0} - \varphi_{GEN12_0}\right) \\ & - \frac{\partial \varphi_{GEN12}}{\partial B_{svc}} Y_{GEN12_0} E_1 E_2 \sin\left(\delta_{1_0} - \delta_{2_0} - \varphi_{GEN12_0}\right)] \end{aligned} \tag{40}$$

$$\begin{aligned} b = \frac{\omega_s}{2H_2}[& -\frac{\partial Y_{GEN22}}{\partial B_{svc}} E_2^2 \cos\left(\varphi_{GEN22_0}\right) \\ & + \frac{\partial \varphi_{GEN22}}{\partial B_{svc}} Y_{GEN22_0} E_2^2 \sin\left(\varphi_{GEN22_0}\right) \\ & - \frac{\partial Y_{GEN21}}{\partial B_{svc}} E_2 E_1 \cos\left(\delta_{2_0} - \delta_{1_0} - \varphi_{GEN21_0}\right) \\ & - \frac{\partial \varphi_{GEN21}}{\partial B_{svc}} Y_{GEN21_0} E_2 E_1 \sin\left(\delta_{2_0} - \delta_{1_0} - \varphi_{GEN21_0}\right)] \end{aligned} \tag{41}$$

$$
\begin{aligned}
c = -\frac{1}{T_{2LP} X_{79}} [& \frac{\partial V_7}{\partial B_{svc}} V_{9_0} \sin\left(\theta_{7_0} - \theta_{9_0}\right) \\
& + \frac{\partial V_9}{\partial B_{svc}} V_{7_0} \sin\left(\theta_{7_0} - \theta_{9_0}\right) \\
& + \frac{\partial \theta_7}{\partial B_{svc}} V_{7_0} V_{9_0} \cos\left(\theta_{7_0} - \theta_{9_0}\right) \\
& - \frac{\partial \theta_9}{\partial B_{svc}} V_{7_0} V_{9_0} \cos\left(\theta_{7_0} - \theta_{9_0}\right)] .
\end{aligned} \tag{42}
$$

Finally, it is clear that the last two parameters *d* and *e* are affected mostly by the values of the PSDC design

$$
\begin{aligned}
d &= \frac{K}{T_2}\left[1 - \frac{T_1}{T_{2LP}}\right] \\
e &= \frac{KT_1}{T_2} c - \frac{1}{T_2} .
\end{aligned} \tag{43}
$$

In next Chapter we will show how the parameters J_{21}, J_{23}, J_{41}, J_{43}, J_{51}, J_{53}, J_{61}, and J_{63} remain constant while the parameters *a*, *b*, and *c* vary when the SVC location changes. We will also see that the *d* and *e* values are modified mostly by the PSDC phase compensation type. By analyzing the parameters *a*, *b*, and *c,* we can then derive rules on the placement of the SVC. Similarly, by studying the properties of the parameters *d* and *e*, we can derive rules on the lead versus lag design principle of the PSDC compensator.

CHAPTER FOUR: TWO-AREA POWER SYSTEM ANALYSIS EXAMPLE

Here, our control strategy is applied to a Two-area Power System as Figure 3.1. In Part 4.1, a series of empirical rules for selecting the power system variables to be monitored by the central control unit are developed and are explained through numerical simulations. In Part 4.2, through an eigenvalue and numerical analysis of the formulation presented in section 3.2, some rules are also obtained for the SVC Local Control Unit.

4.1 DESIGNING THE CENTRAL CONTROL UNIT – OFFLINE RULES

Dynamic simulations are run for different equilibrium points and somewhat different configurations using the Extended Transient-Midterm Stability Program (ETMSP) [45]. A medium disturbance for this system is simulated in order to stimulate the interarea and local modes. At 4.00 seconds, one line from Bus 8 to Bus 9 was disconnected and reconnected after 0.08 seconds. At all cases, the interarea mode and the local modes associated with the generator rotors were all under damped or slightly negative damped. The interarea mode frequency is around 0.5 Hz, and local area 1 and local area 2 modes have very close frequencies of about 1.1 Hz. Simulations were carried out for 25 seconds.

4.1.1 Defining the Time Window

Since Prony analysis is a linear approximation, there is a risk of not getting good estimations during the first strong nonlinear oscillations just after the disturbance has been cleared. When this happen, the estimations obtained from the different signals sets

will not agree and the estimation will be disregarded. The multy-Prony method will then be applied to the next time window.

For the two-area system, Table 4.1 shows relative energy Er_i values of interarea and local modes for two intertie line signals at different time windows. It can be seen that the most dominant mode, the interarea mode, increases its energy about three times with respect to the second most dominant mode when the time window moves from 4.1-8.1 seconds to 5.0-9.0 seconds. Also, Figure 4.1 and Figure 4.2 show how the signal to noise ratio of these two most dominant modes is considerably increased for the same time window change. As a consequence of these results, in this case a time window after the 5^{th} second will allow more accurate estimations than a time window just after the disturbance.

On the other hand, good parameter estimations were achieved by Multi-Prony analysis with only two complete swings of data. Table 4.1, Figure 4.1, and Figure 4.2 show no significant advantages on using a longer time frame in the two area system. However, in a real system, due to more complex dynamics 3 to 4 cycles is a safer option.

Table 4.1 Prony's Ringdown Analysis

Symbol	Signal	*Mode*	f_i	ζ_i	Er_i
	Time Window:		4.1 to 8.1 sec		
P_{78}	Interarea Active Power Flow	Interarea	0.509	0.0000	1.0000
		Local Area 1 or 2	1.088	0.0835	0.0189
V_8	Bus 8 Voltage Magnitude	Interarea	0.508	-0.0048	1.0000
		Local Area 1 or 2	1.110	0.0685	0.0069
	Time Window:		5 to 9 sec		
P_{78}	Interarea Active Power Flow	Interarea	0.508	0.0029	1.0000
		Local Area 1 or 2	1.088	0.0822	0.0066
V_8	Bus 8 Voltage Magnitude	Interarea	0.505	0.0019	1.0000
		Local Area 1 or 2	1.106	0.0677	0.0028
	Time Window:		5 to 13 sec		
P_{78}	Interarea Active Power Flow	Interarea	0.508	0.0002	1.0000
		Local Area 1 or 2	1.087	0.0827	0.0035
V_8	Bus 8 Voltage Magnitude	Interarea	0.509	0.0015	1.0000
		Local Area 1 or 2	1.107	0.0697	0.0015

The Two-area Power System configuration is as Figure 3.1, with an SVCs at Bus 8 operating in voltage regulation form, and with P_{78} =330 MW.

Dynamic Simulation was performed using Extended Transient Midterm Stability Program (ETMSP) from the Electric Power Research Institute (EPRI).

One line from Bus 8 to Bus 9 is removed at 4.00 sec and reconnected at 4.08 sec. Sampling frequency is 62.5 Hz.

Prony signal estimation was calculated using the Ringdown GUI program from BPA/PNNL Dynamic System Identification (DSI) Toolbox. Signal mean values were removed

Mode parameters calculated using the Multi-Area Small Signal Stability Program (MASS) from EPRI are: Interarea Mode, f_i =0.506 and ζ_i =-0.0007; Local Area 1 Mode, f_i =1.078, and ζ_i =0.0638; and Local Area 2 Mode, f_i =1.111, and ζ_i =0.0574.

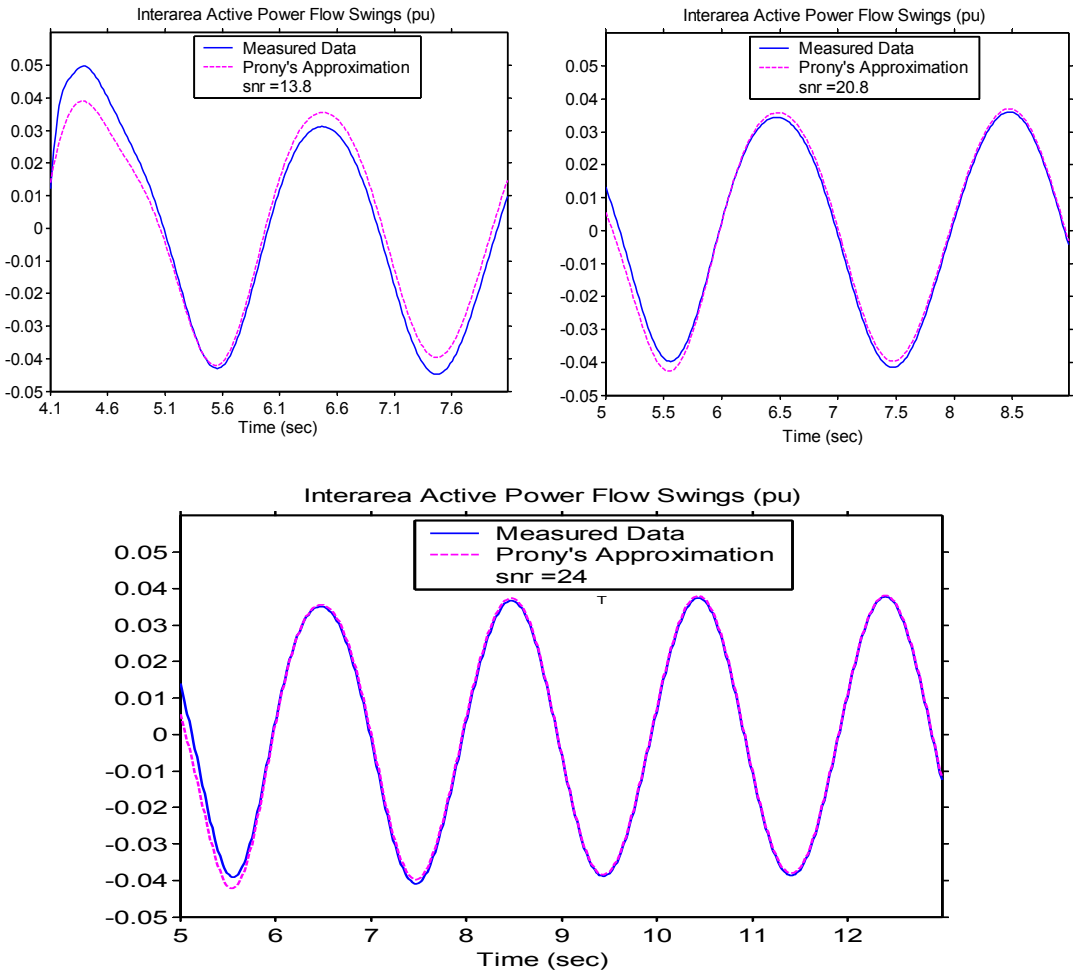

Figure 4.1: Prony's Interarea Active Power Signal Approximation.

Mean Value removed. Interarea and Local modes of Table 4.1 used for the approximation

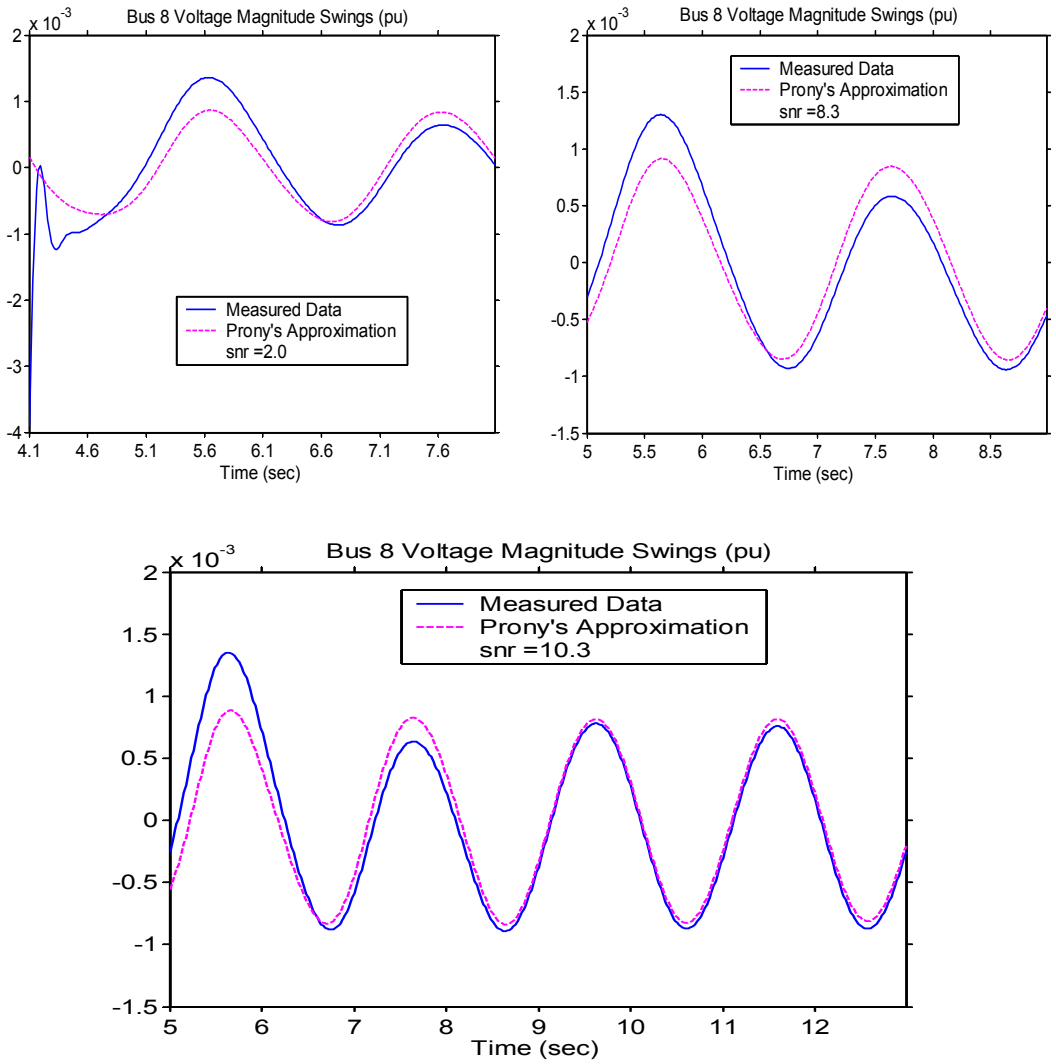

Figure 4.2: Prony's Bus 8 Voltage Magnitude Signal Approximation.

Mean Value removed. Interarea and Local modes of Table 4.1 used for the approximation

4.1.2 Grouping Signals by Dominant Modes

Prony or Multi-Prony analysis of signals with dominant modes that have very close frequencies, as the local area modes in the two-area power system, will likely estimate only one equivalent mode. This could be seen in Table 4.1 on every single signal estimation, and in Table 4.2 on the first two multiple signal estimations, of local area 1 and local area 2 modes. Interarea Active Power Flow P_{78} and Bus 8 Voltage Magnitude V_8 in Table 4.1, are signals that have interarea and local area mode content of the two local modes. However, Prony analysis is not able to distinguish between the two local modes.

Table 4.2: Multi-Prony Analysis
Case I
(Signals with Different Dominant Modes Combined)

Signals	Least Square Solution	*Mode*	f_i	ζ_i
θ_8, δ_2, and δ_4	Singular Value Decomposition	Interarea	0.521	0.0164
		Local Area 1 or 2	1.104	0.0710
I_{78}, I_{67}, and I_{910}	Singular Value Decomposition	Interarea	0.564	-0.1920
		Local Area 1 or 2	1.079	-0.0560
I_{78}, I_{67}, and I_{910}	Total Least Squares	Interarea	0.525	0.0143
		Local Area 1	1.066	0.0332
		Local Area 2	1.302	0.0948

Same signal measurements and programs as Table 4.3

In Table 4.2, we present a multi-Prony analysis of two different groups of signals. Both groups include signals that have different dominant modes. In the first group, the generator 2 rotor angle, δ_2 has local area 1 mode and interarea mode as dominant modes, while the generator 4 rotor angle, δ_4 have local area 2 mode and interarea mode as dominant modes. In the second group, line 6 to 7 current magnitude I_{67} has local area 1 mode and interarea mode as dominant modes, and line 9 to 10 current magnitude I_{910} has

local area 2 mode and interarea mode as dominant modes. However, multi-Prony analysis at the first two rows fails on the estimation of the two local modes and gives an equivalent estimation of only one mode.

The estimation problem of modes with very close frequencies may be addressed by analyzing signals that are predominantly affected by only one of these modes. For this case, we may see in Table 4.3 and Table 4.4 how analyzing signals grouped by local area modes and by interarea modes give a clear estimation of each mode. Therefore, observability is improved by classifying signals by dominant modes in groups and analyzing them independently.

Table 4.3: Prony Mode Parameter Estimation

Case 1

(Signals Grouped by Dominant Modes)

Symbol	Signal	A_i	f_i	ζ_i	Ar_i
	Interarea Mode [a]		0.523	0.0111	
I_{78}	Interarea Current Magnitude	0.224	0.524	0.0143	1.000
P_{78}	Interarea Active Power Flow	0.156	0.522	0.0177	1.000
Q_{78}	Interarea Reactive Power Flow	0.061	0.520	0.0183	1.000
V_6	Bus 6 Voltage Magnitude	0.015	0.524	0.0176	1.000
V_8	Bus 8 Voltage Magnitude	0.018	0.521	0.0167	1.000
V_{10}	Bus 10 Voltage Magnitude	0.009	0.519	0.0177	1.000
θ_{10}	Bus 10 Voltage Angle	2.461	0.522	0.0178	0.761
θ_8	Bus 8 Voltage Angle	1.522	0.520	0.0181	0.652
θ_6	Bus 6 Voltage Angle	0.076	0.559	-0.0143	0.068
	Local Area 1 Mode [a]		1.090	0.0694	
δ_1	Generator 1 Rotor Angle	0.163	1.084	0.1113	0.145
I_{67}	Line 6 to 7 Current Magnitude	0.009	1.081	0.0558	0.033
θ_6	Bus 6 Voltage Angle	0.033	1.074	0.0582	0.030
δ_2	Generator 2 Rotor Angle	0.170	1.083	0.0753	0.031
V_1	Bus 1 Voltage Magnitude	2e-4	1.041	0.0529	0.027
V_2	Bus 2 Voltage Magnitude	1e-4	1.100	0.0062	0.008
V_6	Bus 6 Voltage Magnitude	1e-4	1.075	-0.0032	0.007
	Local Area 2 Mode [a]		1.118	0.0704	
I_{910}	Line 9 to 10 Current Magnitude	0.011	1.060	0.0356	0.071
δ_4	Generator 4 Rotor Angle	0.153	1.120	0.0718	0.056
V_3	Bus 3 Voltage Magnitude	2e-4	1.207	0.0847	0.029
δ_3	Generator 3 Rotor Angle	0.080	1.142	0.0672	0.028
V_{10}	Bus 10 Voltage Magnitude	2e-4	1.249	0.1213	0.024
θ_{10}	Bus 10 Voltage Angle	0.029	1.143	0.0748	0.009
V_4	Bus 4 Voltage Magnitude	3e-4	1.226	0.1551	0.004

The Two-area Power System configuration is as Figure 3.1, without SVCs, with only two lines from Bus 8 to Bus 9, and with P_{78} =400 MW.

Dynamic Simulation was performed using Extended Transient Midterm Stability Program (ETMSP) from the Electric Power Research Institute (EPRI).

One line from Bus 8 to Bus 9 is removed at 4.00 sec and reconnected at 4.08 sec. Sample data is taken from 5.00 sec to 9.00 sec. Sampling frequency is 62.5 Hz.

Prony and Multi-Prony signal estimation was calculated using the Ringdown GUI program from BPA/PNNL Dynamic System Identification (DSI) Toolbox. Signal mean values were removed.

[a] Values calculated using the Multi-Area Small Signal Stability Program (MASS) from EPRI.

Table 4.4: Prony Mode Parameter Estimation

Case2

(Signals Grouped by Dominant Modes)

Symbol	Signal	A_i	f_i	ζ_i	Ar_i
	Interarea Mode [a]		0.506	-0.0007	
I_{78}	Interarea Current Magnitude	0.045	0.506	-0.0010	1.000
P_{78}	Interarea Active Power Flow	0.039	0.508	0.0029	1.000
Q_{78}	Interarea Reactive Power Flow	0.008	0.506	0.0029	1.000
V_6	Bus 6 Voltage Magnitude	0.002	0.485	0.0405	1.000
V_8	Bus 8 Voltage Magnitude	9e-4	0.505	0.0019	1.000
V_{10}	Bus 10 Voltage Magnitude	4e-4	0.504	-0.0225	0.266
θ_{10}	Bus 10 Voltage Angle	0.296	0.506	0.0096	0.226
θ_8	Bus 8 Voltage Angle	0.131	0.496	0.0196	0.132
θ_6	Bus 6 Voltage Angle	0.152	0.511	-0.0067	0.115
	Local Area 1 Mode [a]		1.078	0.0638	
V_1	Bus 1 Voltage Magnitude	1e-4	1.058	0.1058	0.136
I_{67}	Line 6 to 7 Current Magnitude	0.006	1.093	0.0806	0.125
δ_1	Generator 1 Rotor Angle	0.086	1.083	0.0904	0.067
δ_2	Generator 2 Rotor Angle	0.111	1.078	0.0885	0.039
V_6	Bus 6 Voltage Magnitude	6e-5	1.038	0.0444	0.029
θ_6	Bus 6 Voltage Angle	0.027	1.076	0.0927	0.021
V_2	Bus 2 Voltage Magnitude	5e-6	1.438	-0.1191	2e-4
	Local Area 2 Mode [a]		1.111	0.0574	
V_3	Bus 3 Voltage Magnitude	2e-4	1.105	0.0687	0.152
δ_4	Generator 4 Rotor Angle	0.109	1.098	0.0735	0.148
I_{910}	Line 9 to 10 Current Magnitude	0.006	1.084	0.0806	0.146
V_{10}	Bus 10 Voltage Magnitude	2e-4	1.103	0.0668	0.129
V_4	Bus 4 Voltage Magnitude	1e-4	1.103	0.0660	0.074
δ_3	Generator 3 Rotor Angle	0.079	1.103	0.0738	0.060
θ_{10}	Bus 10 Voltage Angle	0.030	1.098	0.0710	0.023

The Two-area Power System configuration is as Figure 3.1, with an SVCs at Bus 8 operating in voltage regulation form, and with P_{78} =330 MW.

Dynamic Simulation was performed using Extended Transient Midterm Stability Program (ETMSP) from the Electric Power Research Institute (EPRI).

One line from Bus 8 to Bus 9 is removed at 4.00 sec and reconnected at 4.08 sec. Sample data is taken from 5.00 sec to 9.00 sec. Sampling frequency is 62.5 Hz.

Prony and Multi-Prony signal estimation was calculated using the Ringdown GUI program from BPA/PNNL Dynamic System Identification (DSI) Toolbox. Signal mean values were removed.

[a] Values calculated using the Multi-Area Small Signal Stability Program (MASS) from EPRI.

4.1.3 Using Mode Content: Group using A_i and Ar_i

It is clear from Table 4.3 and Table 4.4 that signals with the greatest dominant mode content are the more likely to give the best estimations. However, even with these signals it is still possible to have bad estimations when using Prony analysis. It has been proof in [37] that using multi-Prony will increase the accuracy of the estimations, but still due to the nonlinear nature of Power System signals we may have bad estimations. Our goal with this rule is making as many subgroups as we want in order to increase the redundancy level in our estimations divided by dominant modes.

When using Prony's method (14), amplitude A_i is a good approximation of mode ***i*** content in the processed signal. However, signals have very different value ranges even in per unit basis. Therefore, it is important considering the relative amplitude Ar_i, when judging the real mode content on a signal. In Table 4.3 and Table 4.4, signals like voltage magnitudes V_1, V_2, V_4 and V_6, and Bus voltage angle θ_6 in Table 4.3, and V_1, V_2, V_{10}, V_6, and θ_8 in Table 4.4 are between the signals with the lowest A_i and Ar_i values at each group and are the ones with the largest estimation differences with respect to the damping ratio calculated with the Multi-Area Small Signal Stability (MASS) Program.

Combining signals that have high A_i and Ar_i values with fewer signals that have low A_i or Ar_i values may improve the general estimation, as it is the case for the group formed by θ_{10}, θ_8, and θ_6, and the group formed by δ_2, I_{67}, and V_6 in Table 4.5. In most cases, relative amplitude Ar_i is increased when using multi-Prony analysis of signals with similar dominant modes, as seen in Table 4.5 and Table 4.6. On the other hand, Multi-Prony's method for analyzing signal sets where all signals have very low A_i and Ar_i values does not improve the estimation, as it is the case for the group of voltage magnitudes V_1, V_2, and V_6 in Table 4.5.

Table 4.5: Multi-Prony Mode Parameter Estimation

Case 1

(Signals Grouped by Dominant Modes)

Symbol	Signal	A_i	f_i	ζ_i	Ar_i
	Interarea Mode [a]		0.523	0.0111	
V_6,		0.015			1.000
V_8,		0.018	0.522	0.0199	1.000
and V_{10}		0.010			1.000
θ_{10},		2.488			0.202
θ_8,		1.534	0.522	0.0191	0.124
and P_{78}		0.152			1.000
θ_{10},		2.454			1.000
θ_8,		1.490	0.525	0.0189	0.815
and θ_6		0.175			0.095
	Local Area 1 Mode [a]		1.090	0.0694	
V_1,		9e-5			0.009
V_2,		7e-5	1.058	-0.0107	0.005
and V_6		9e-5			0.006
δ_2,		0.173			0.117
I_{67},		0.011	1.082	0.0765	0.040
and θ_6		0.040			0.028
δ_2,		0.173			0.145
I_{67},		0.011	1.083	0.0765	0.041
and V_6		2e-4			0.012
	Local Area 2 Mode [a]		1.118	0.0704	
δ_4		0.153	1.120	0.0718	0.056
and V_3		3e-4			0.046
I_{910},		0.012			0.085
δ_3,		0.177	1.077	0.1048	0.057
and V_{10}		7e-4			0.074
I_{910},		0.018			0.122
δ_3,		0.086	1.140	0.0705	0.030
and θ_{10}		0.021			0.009

Same signal measurements and programs as Table 4.3

Table 4.6: Multi-Prony Mode Parameter Estimation

Case 2

(Signals Grouped by Dominant Modes)

Symbol		A_i	f_i	ζ_i	Ar_i
	Interarea Mode [a]		0.506	-0.0007	
V_6,		0.002			1.000
V_8,		9e-4	0.506	0.0055	0.562
and V_{10}		5e-4			0.242
I_{78}, P_{78}, and V_6	(SVD)		(No Good Estimations)		
I_{78}, P_{78}, and V_6	(TLS)		(No Good Estimations)		
I_{78},		0.047			1.000
P_{78},	(QR Factorization)	0.039	0.508	0.0024	1.000
and V_6		0.002			1.000
θ_{10},		0.282			0.167
θ_8,		0.108	0.508	0.0063	0.065
and θ_6		0.168			0.102
	Local Area 1 Mode [a]		1.078	0.0638	
δ_1		0.102	1.081	0.0952	0.064
and V_1		5e-4			0.491
δ_2,		0.110			0.065
I_{67},		0.006	1.077	0.0885	0.133
and θ_6		0.025			0.015
δ_2,		0.111			0.058
I_{67},		0.006	1.078	0.0887	0.130
and V_2		5e-5			0.038
	Local Area 2 Mode [a]		1.111	0.0574	
δ_4		0.109	1.098	0.0734	0.141
and V_3		4e-4			0.177
I_{910},		0.005			0.126
δ_3,		0.076	1.105	0.0687	0.024
and V_{10}		2e-4			0.093

Same signal measurements and programs as Table 4.4

4.1.4 Validating the groups

With this rule we want to select the final subgroups that are going to be used for monitoring the mode shape of our Power System in real time. While we want to have a good redundancy level on the estimation of each mode, we also want to make sure that the chosen subgroups has the ability of providing good estimations of the excited modes when a small or medium disturbance occurs in the Power System.

Since Prony or multi-Prony analysis is a linear approach applied to nonlinear signals, we should expect certain margin of error in estimations from different signals during the same time-window. Therefore, an acceptable error margin α should be defined in order to admit or not the estimations. In Table 4.5, for example, an accuracy level α of ± 0.01 with respect to the mode damping ratio values found with the Multi-Area Small Signal Stability (MASS) Program may be selected. In consequence, the estimation from the group of voltage magnitudes V_1, V_2, and V_6 will be considered as a bad estimation and will be eliminated as a subgroup.

Crosschecking damping ratio values obtained from subgroups selected according with rules 1, 2, and 3, is another way on determining the final subgroups if no actual mode value is known. According with our results in the Two-Area and the WSCC Power Systems, a difference α of $\pm 2\%$ damping ratio value between the minimum and the maximum estimation for one damping ratio may be acceptable. Bad groups, or groups with signals with weak contain of certain mode will be discarded as they are detected with the crosschecking process.

Nevertheless, it is important to take in mind that good data that fulfill the best conditions of the above rules may give bad results. This can be seen in Table 4.2 and Table 4.6 for the second group of signals, where in spite of being part of the signals with higher amplitudes and relative amplitudes at each group in Table 4.3 and Table 4.4 respectively, we do get completely unacceptable results at the first attempt of solving the

least square problem. The results have shown that changing the least square solution method originally used for the bad estimation will contribute to solve the problem for these cases, as shown in Table 4.2, Table 4.6 , and Table 5.3 in the WSCC application example.

4.2 THE SVC LOCAL CONTROL UNIT

Two types of SVC PSDC modes are compared against an SVC in voltage regulation form, for a three phase fault in one of the lines that goes from bus 8 to bus 9 in the Two-area Power System. The first one is an SVC operating on local voltage regulation as primary control mode and including a remote interarea active power flow signal as input for a PSDC supplementary control, [21]. The second SVC control type is a full PSDC with interarea active power flow as input signal. The controllers are compared on the basis of interarea power damping, at different locations and at different operating conditions. From these simulations, we have observed that an SVC working on full PSDC mode is a more effective way to increase damping of power interarea oscillations for emergency situations. Figure 4.3 shows some typical results. Similar conclusion was also reached at [4]. Additional tests have also showed that in case of uncoordinated control actions, only one SVC in full PSDC gives better results than two or more SVC acting on the same mode.

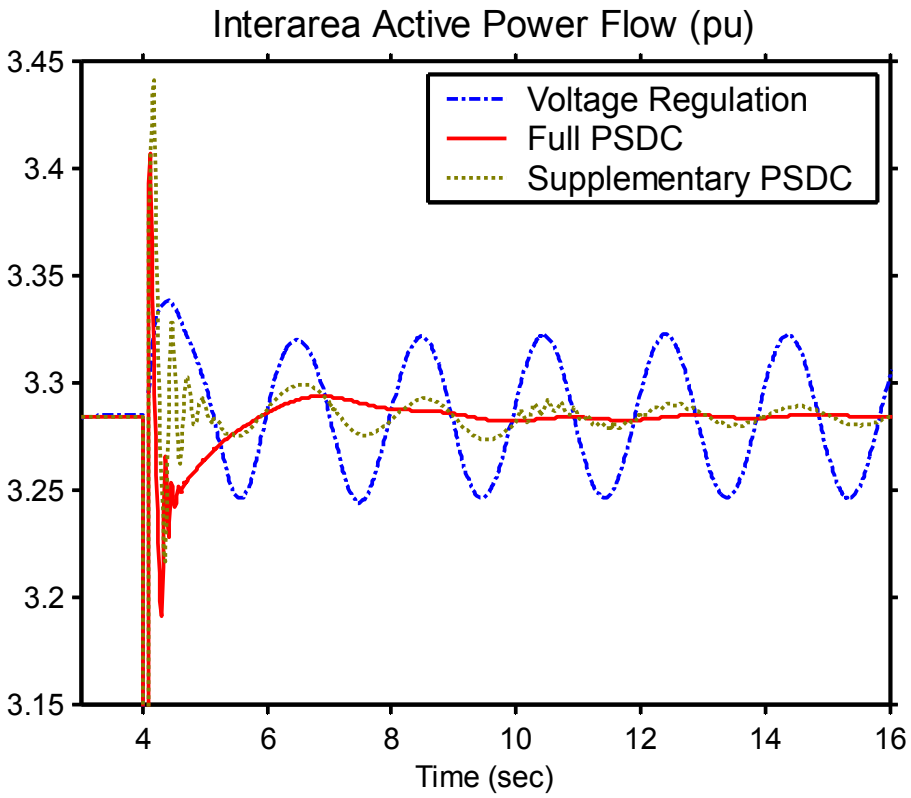

Figure 4.3: Three SVC control types (SVC at bus 8)

Next, the effects of SVC location and full PSDC phase compensation on the Jacobian matrix parameters and on the system eigenvalues are analyzed. Using the classical representation described in section 3.2.2, we identify the **J** matrix parameters that are more significantly affected by the SVC location and phase compensation variables. Then, we study the resulting behavior of those parameters and their effect on the associated eigenvalues and on the small signal stability of the system. Finally, additional simulation results from an available commercial software package are presented. They include simulations on the reduced Two-area Power System and on the full Two-area Power System represented in Figure 3.1 with two-axis models, exciters and nonlinear load representation.

4.2.1 Matlab Results using a Classical Model

The Jacobian matrix $\mathbf{J}_{nosvc}$, the eigenvalues $\boldsymbol{\lambda}_{nosvc}$, and the participation factors matrix $\mathbf{P}_{nosvc}$, obtained for a reduced Two-area Power System without SVC's and with only two generators, are shown in Figure 4.4. It is clear from the participation matrix $\mathbf{P}_{nosvc}$ that eigenvalues $\lambda_{1,2} = -0.0198 \pm 7.2144\text{i}$ are equitably related with the rotor state variables at the two areas. Therefore, they determine the interarea mode of this system. The calculated interarea mode frequency and damping ratio for this case are: $f_{1,2} = 1.1482$ in Hz and $\zeta_{1,2} = 0.0027$.

$$\mathbf{J}_{nosvc} = \begin{bmatrix} 0 & 1.0000 & 0 & 0 \\ -21.0094 & -0.0385 & 21.0097 & 0 \\ 0 & 0 & 0 & 1.0000 \\ 31.0386 & 0 & -31.0383 & -0.0405 \end{bmatrix} \qquad \mathbf{x}_{0\_nosvc} = \begin{bmatrix} 0.3500 \\ 0 \\ 0.2000 \\ 0 \end{bmatrix}$$

$$\mathbf{P}_{nosvc} = \begin{bmatrix} 0.2018 & 0.2018 & 0.5136 & 0.0827 \\ 0.2018 & 0.2018 & 0.0734 & 0.5230 \\ 0.2982 & 0.2982 & 0.3633 & 0.0403 \\ 0.2982 & 0.2982 & 0.0497 & 0.3540 \end{bmatrix} \qquad \boldsymbol{\lambda}_{nosvc} = \begin{bmatrix} -0.0198+7.2144\text{i} \\ -0.0198-7.2144\text{i} \\ 0.0064 \\ -0.0457 \end{bmatrix}$$

Figure 4.4: Two-area Power System Without SVC. K_D=0.5. Matlab Mode

Figure 4.5 shows the Jacobian matrices $\mathbf{J}_{svcB7\_LP}$, $\mathbf{J}_{svcB8\_LP}$, $\mathbf{J}_{svcB9\_LP}$ of the reduced Two-area Power System above with an SVC located at bus 7, bus 8, and bus 9 respectively. The SVC's are in PSDC mode and the controller includes a low pass filter and a zero phase compensator (32). Notice that as described in (36) and (37), the submatrix related with the original system without SVC's does not change with the addition of the SVC's. This is because the change in the admittance $\mathbf{Y}_{GEN}$ matrix is too small when an SVC is added. Therefore, values included into this submatrix do not have

any significant effect in the mode shape variation that takes place when an SVC working in full PSDC is included into the system.

$$\mathbf{J}_{svcB7\_LP} = \begin{bmatrix} 0 & 1.0000 & 0 & 0 & 0 & 0 \\ -21.0094 & -0.0385 & 21.0097 & 0 & 0 & -6.8474 \\ 0 & 0 & 0 & 1.0000 & 0 & 0 \\ 31.0386 & 0 & -31.0383 & -0.0405 & 0 & -3.4187 \\ -17.7602 & 0 & 17.7603 & 0 & -6.2500 & -0.2337 \\ -17.7602 & 0 & 17.7603 & 0 & 0.0332 & -6.5168 \end{bmatrix}$$

$$\mathbf{J}_{svcB7\_LP} = \begin{bmatrix} 0 & 1.0000 & 0 & 0 & 0 & 0 \\ -21.0094 & -0.0385 & 21.0097 & 0 & 0 & -6.8474 \\ 0 & 0 & 0 & 1.0000 & 0 & 0 \\ 31.0386 & 0 & -31.0383 & -0.0405 & 0 & -3.4187 \\ -17.7602 & 0 & 17.7603 & 0 & -6.2500 & -0.2337 \\ -17.7602 & 0 & 17.7603 & 0 & 0.0332 & -6.5168 \end{bmatrix}$$

$$\mathbf{J}_{svcB7\_LP} = \begin{bmatrix} 0 & 1.0000 & 0 & 0 & 0 & 0 \\ -21.0094 & -0.0385 & 21.0097 & 0 & 0 & -6.8474 \\ 0 & 0 & 0 & 1.0000 & 0 & 0 \\ 31.0386 & 0 & -31.0383 & -0.0405 & 0 & -3.4187 \\ -17.7602 & 0 & 17.7603 & 0 & -6.2500 & -0.2337 \\ -17.7602 & 0 & 17.7603 & 0 & 0.0332 & -6.5168 \end{bmatrix}$$

Figure 4.5: The **J** matrix with SVC compensation at Bus 7, Bus 8, and Bus 9. The SVC control includes a Low Pass Filter and a 0° phase compensator. K_D=0.5. Matlab Model.

On the other hand, the values of parameters *a*, *b*, and *c* change with respect to the SVC location at any of the two areas or along the intertie line. Table 4.7 shows these parameter value variations when an SVC is located in buses 7, 8, and 9. From (40), (41), and (42) and the approximations we have made; changes in *a*, *b*, and *c* parameter values,

when moving from one side to the other, depend mostly on the changes suffered by admittance sensitivities. Between them, parameter *c* value is the one that experienced the smaller changes and therefore, has little effect on the observed differences in the interarea mode damping.

Table 4.7: Two Area Power System [a]

Matlab Results

SVC Location	PSDC Compensation (Low Pass filter +)	*a*	*b*	*c*	*d*	*e*	$\lambda_{1,2}$	*f*	ζ
No SVC	-	-	-	-	-	-	-0.0198 ± 7.2144i	1.1482	0.0027
Bus 7	LP filter only	-6.847	-3.418	-0.233	0.033	-6.516	-0.3778 ± 6.9144i	1.1005	0.0546
	LP filter + 15° lag				2.083	-4.995	-0.5799 ± 6.9947i	1.1132	0.0826
	LP filter + 30° lag				5.514	-3.567	-0.8169 ± 7.2296i	1.1506	0.1123
	LP filter + 45° lag				10.416	-2.614	-0.9890 ± 7.5595i	1.2031	0.1297
	LP filter + 15° lead				-1.488	-8.567	-0.2142 ± 6.9133i	1.1003	0.0310
	LP filter + 30° lead				-2.916	-11.998	-0.0838 ± 6.9651i	1.1085	0.0120
	LP filter + 45° lead				-3.869	-16.900	-0.0196 ± 7.0295i	1.1188	0.0028
Bus 8	LP filter only	-5.406	-5.967	-0.411	0.033	-6.694	0.0311 ± 7.2620i	1.1558	-0.0043
	LP filter + 15° lag				2.083	-5.173	0.0583 ± 7.2571i	1.1550	-0.0080
	LP filter + 30° lag				5.514	-3.745	0.0997 ± 7.2416i	1.1525	-0.0138
	LP filter + 45° lag				10.416	-2.792	0.1523 ± 7.2169i	1.1486	-0.0211
	LP filter + 15° lead				-1.488	-8.745	0.0095 ± 7.2608i	1.1556	-0.0013
	LP filter + 30° lead				-2.916	-12.176	-0.0093 ± 7.2536i	1.1544	0.0013
	LP filter + 45° lead				-3.869	-17.078	-0.0195 ± 7.2441i	1.1529	0.0027
Bus 9	LP filter only	-3.263	-7.429	-0.580	0.033	-6.863	0.3219 ± 7.5536i	1.2022	-0.0426
	LP filter + 15° lag				2.083	-5.342	0.4888 ± 7.5412i	1.2002	-0.0647
	LP filter + 30° lag				5.514	-3.913	0.7430 ± 7.5030i	1.1941	-0.0985
	LP filter + 45° lag				10.416	-2.961	1.0590 ± 7.4738i	1.1895	-0.1403
	LP filter + 15° lead				-1.488	-8.913	0.1850 ± 7.5416i	1.2003	-0.0245
	LP filter + 30° lead				-2.916	-12.345	0.0594 ± 7.4954i	1.1929	-0.0079
	LP filter + 45° lead				-3.869	-17.247	-0.0137 ± 7.4315i	1.1828	0.0018

[a] This is a Reduced Two-area Power System , with only two generators, the SVC consists only of a Low Pass Filter and a Lead or Lag Filter, K_D =0.5, P_{78} =90 MW.

Results were calculated using a designed Matlab model.

Admitance sensitivities for an SVC at bus 7, 8, or 9 were found for a positive step in its B_{svc} bus output value (32). These sensitivities are shown in Figure 4.6, as well as the variation suffered by each of the four right terms in *a* and *b* formulations, (40) and (41).

If we compare corresponding sensitivities in *a* and *b* terms, sensitivities $\frac{\partial \varphi_{GEN11}}{\partial B_{svc}}$ and $\frac{\partial \varphi_{GEN22}}{\partial B_{svc}}$ are the only sensitivity factors with opposite slopes when moving the SVC from the sending area to the receiving area, through the intertie. Therefore, they are the main cause of the value difference between second right terms of *a* and *b* expressions, called here a_{sr} and b_{sr}, and ultimately for the value difference between terms *a* and *b*. We may say here, that the difference between *a* and *b* values is a deterministic characteristic of the SVC location in PSDC mode.

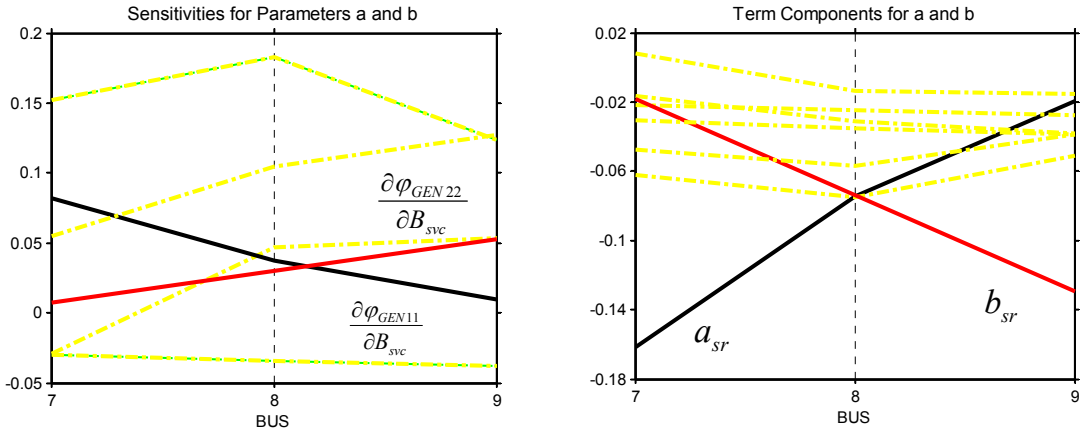

Figure 4.6: Sensitivities and term component variations in *a* and *b*

In this particular matlab model, the value difference term, *b-a,* is positive when the SVC is at the sending side, almost zero if the SVC is located close to the center of the intertie line, and negative if the SVC is at the receiving side. Also, we note that the greater the absolute value difference between *a* and *b*, the greater the stabilizing or destabilizing capacity of the SVC in full PSDC. This could be seen in Figure 4.7 for phase-lag compensation. Also, in Table 4.7 and Table 4.9 this phenomenon may be

observed when comparing the stabilizing and destabilizing effects of the SVC's in buses 7 and 9 with respect to an SVC in bus 8.

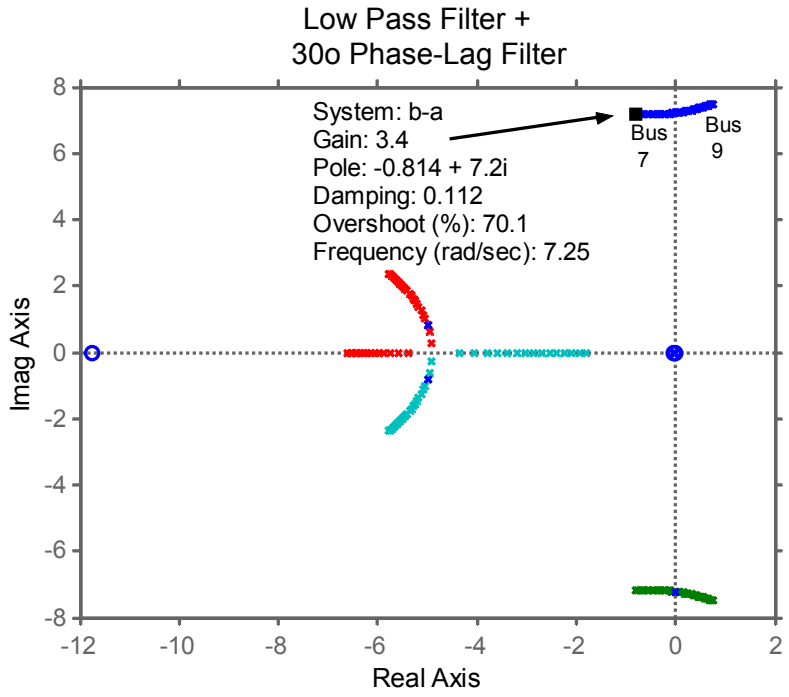

Figure 4.7: Root Locus with respect to *b-a*.

The Gain is: $-4.2 \le b - a \le 3.4$.

Additionally, we have parameters *d* and *e* (43) that depend on the SVC's controller specifications and on parameter *c*, which does not change much in this study. Therefore as seen in Table 4.7, parameters *d* and *e* have similar values at buses 7, 8, and 9, since they vary mostly with the type of PSDC compensation used and not with SVC location. Notice that in order to obtain comparative results and avoid the gain *K* effect in *d* and *e* values, we set $K = T_2/T_1$. As may be seen in (43), with $K = T_2/T_1$, *d* depends mostly on T_1 while *e* mostly on T_2; the magnitudes of *d* and *e* vary inversely proportional to T_1 and T_2, respectively. That is, *d* magnitude increases when interarea active power phase-lag

compensation increases and *e* magnitude does the same, when phase-lead compensation is increased.

Figures Figure 4.8, Figure 4.9, and Figure 4.10, show the effect on the root locus of *d* value in phase-lag compensation and *e* value in phase-lead compensation for buses 7, 8, and 9. From these figures and Table 4.7, it is clear that: intensification of interarea active power phase-lag compensation, or *d* magnitude increment, is particularly beneficial on increasing the interarea mode damping for an SVC located at the sending area, as bus 7; while it is disadvantageous when the SVC is located at the receiving area, as bus 9. However, it is important to note that increasing *d* too much in bus 7, could lead to another pole close to the imaginary axis moves to the right hand side attracted by a zero at this side. Alternatively, the intensification of phase-lead compensation has a good effect on damping the interarea mode when the SVC is located at the receiving area and an opposite effect, when located at the sending side. For an SVC close to the middle of the intertie line, as bus 8, the effects are much lower.

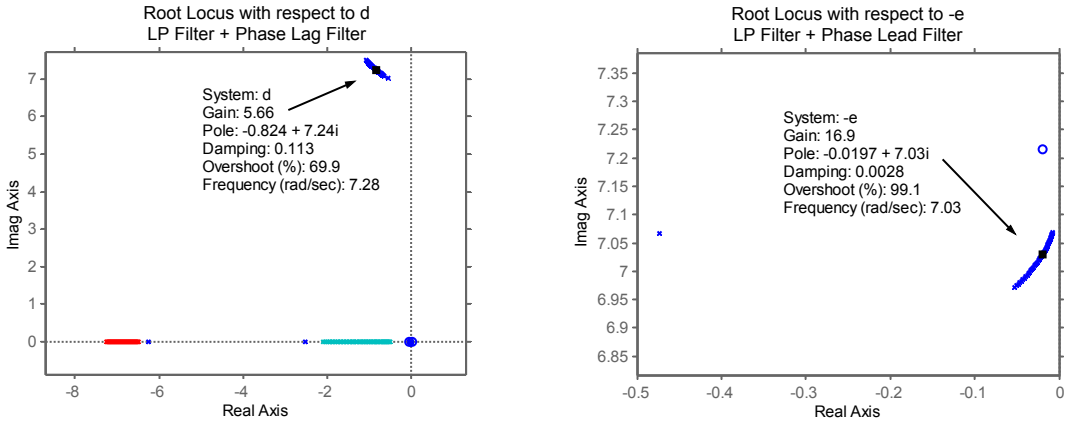

Figure 4.8: Root Locus for the SVC at Bus 7.

The Gains are: : $2 \le d \le 12$ and $-12 \ge e \ge -22$

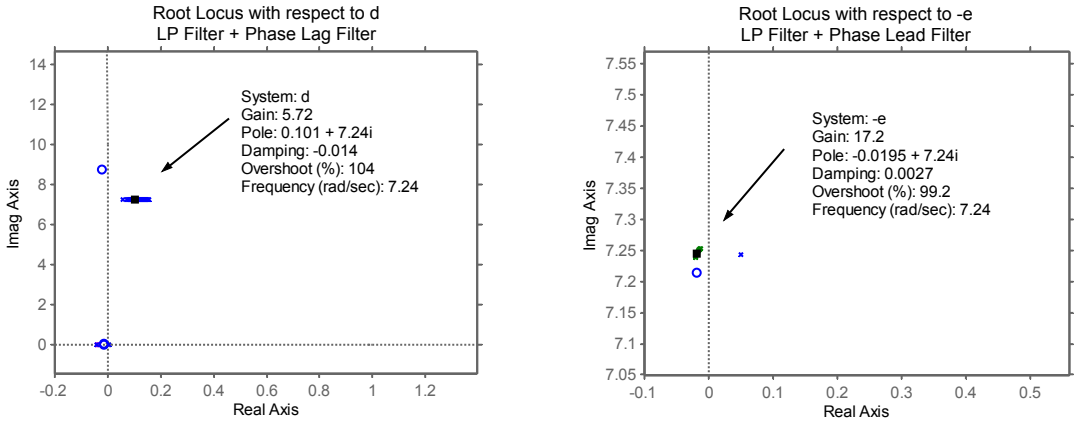

Figure 4.9: Root Locus for the SVC at Bus 8.

The Gains are: $2 \le d \le 12$ and $-12 \ge e \ge -22$

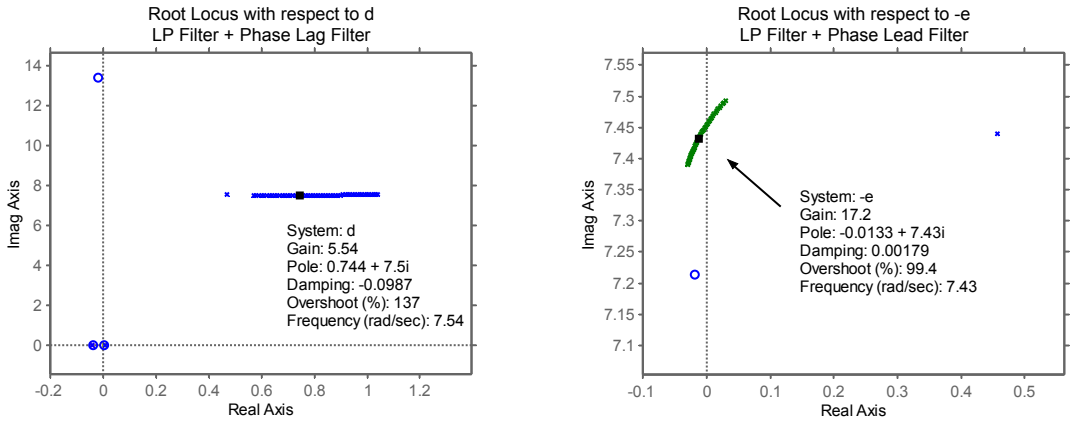

Figure 4.10: Root Locus for the SVC at Bus 9.

The Gains are: $2 \le d \le 12$ and $-12 \ge e \ge -22$

Based on the above analysis and numerical results, we may say that parameters *a* and *b* values have the biggest impact on damping interarea modes with an SVC in full PSDC operation. That is, location of the SVC is the most important factor to consider in this kind of control. Then, based on the SVC location, the interarea active power phase compensation should be decided, setting the *d* and *e* values.

As seen from the above and the following results, *the most effective location for an SVC in full interarea active PSDC mode is the sending side.*

If we are interested in selecting the best bus location into either the sending or receiving area for the SVC control, admittance sensitivities should be considered and the greater absolute value difference term *b-a* should determine the best SVC full PSDC location in that area.

4.2.2 MASS Results

In this subsection, the EPRI small-signal stability program, Multi-Area Small Signal Stability (MASS) software package [45] is used to double check the eigenvalue results of the previous section. We use first the included classical model for the reduced Two-area Power System and second, a two-axis generator model of the full system represented in Figure 3.1, including exciters, speed governors and no-linear load modeling. These results are presented in Table 4.8 and Table 4.9. The results suggest that the conclusions obtained from our reduced mathematical model may be extended to more complex systems.

Notice that, *a* and *b* values in Table 4.8 are consistent with *a* and *b* values in Table 4.7. The absolute value for *a* is always greater than the absolute value of *b* at the sending area, while the relation is the opposite when moving to the receiving area. Phase-lag compensation improves interarea mode damping and phase-lead reduces damping, at the

sending side. The opposite phenomena may be observed at the receiving side. For bus 8, which is almost at the center between areas 1 and 2, these differences are reduced.

Nevertheless, we notice that in the reduced classical model, bus 8 results are more comparable to those of the sending side; while, in the full system model, bus 8 results are closer to those of the receiving side. Since, at bus 8 the value difference between bus angle admittance sensitivities $\frac{\partial \varphi_{GEN11}}{\partial B_{svc}}$ and $\frac{\partial \varphi_{GEN22}}{\partial B_{svc}}$ is very small, a small change in the system configuration makes the bus move from one side to the other for PSDC issues.

Table 4.8: Two Area Power System

Mass Results – *a* and *b* values

SVC Location	PSDC Compensation (Low Pass filter +)	Reduced Classical Model [a]		Full Two-axis Model [b]			
		a	*b*	a_1 [c]	a_2 [c]	b_3 [c]	b_4 [c]
Bus 7	LP filter only	0.13e-3	0.63e-4	0.38e-4	0.55e-4	0.87e-5	0.33e-5
	LP filter + 15° lag	1.717	0.856	0.519	0.749	0.120	0.046
	LP filter + 30° lag	2.871	1.431	0.868	1.252	0.200	0.077
	LP filter + 45° lag	3.434	1.712	1.038	1.497	0.239	0.092
	LP filter + 15° lead	-3.005	-1.498	-0.909	-1.310	-0.209	-0.080
	LP filter + 30° lead	-10.13	-5.052	-3.064	-4.418	-0.706	-0.271
	LP filter + 45° lead	-24.04	-11.98	-7.268	-10.48	-1.675	-0.643
Bus 8	LP filter only	0.97e-4	0.11e-3	0.31e-4	0.49e-4	0.30e-4	0.30e-4
	LP filter + 15° lag	1.323	1.486	0.424	0.669	0.409	0.417
	LP filter + 30° lag	2.213	2.485	0.709	1.119	0.684	0.697
	LP filter + 45° lag	2.647	2.972	0.848	1.338	0.818	0.834
	LP filter + 15° lead	-2.316	-2.600	-0.742	-1.171	-0.715	-0.730
	LP filter + 30° lead	-7.811	-8.769	-2.502	-3.950	-2.413	-2.460
	LP filter + 45° lead	-18.53	-20.80	-5.936	-9.368	-5.723	-5.836
Bus 9	LP filter only	0.57e-4	0.14e-3	0.14e-4	0.23e-4	0.45e-4	0.57e-4
	LP filter + 15° lag	0.775	1.847	0.198	0.317	0.615	0.774
	LP filter + 30° lag	1.296	3.088	0.331	0.529	1.028	1.294
	LP filter + 45° lag	1.550	3.693	0.396	0.633	1.229	1.547
	LP filter + 15° lead	-1.356	-3.231	-0.347	-0.554	-1.076	-1.354
	LP filter + 30° lead	-4.573	-10.900	-1.170	-1.869	-3.627	-4.566
	LP filter + 45° lead	-10.85	-25.85	-2.775	-4.433	-8.604	-10.83

[a] This is a Reduced Two-area Power System model of Fig. 3, with only two generators, the SVC consists of a Low Pass Filter, a Lead or Lag Filter, and an Static Device #1 End Block [31], K_D =0.5, P_{78} =165 MW.

[b] This is a Full Two-area Power System model of Fig. 3, exciters are included, the SVC consists of a Low Pass Filter, a Lead or Lag Filter, and an Static Device #1 End Block [31], K_D =0.0, P_{78} =330 MW.

[c] a_1, a_2 are for generators 1 and 2 at the sending area. b_3, b_4 are for generators 3 and 4 at the receiving area.

Results were calculated using the Multi-Area Small Signal Stability Program (MASS) from EPRI.

Table 4.9: Two Area Power System

MASS Results

SVC Location	PSDC Compensation (Low Pass filter +)	Reduced Classical Model [a]			Full Two-axis Model [b]		
		$\lambda_{1,2}$	f	ζ	$\lambda_{1,2}$	f	ζ
No SVC	-	-0.0198±3.771i	0.600	0.005	-0.0047±3.167i	0.504	0.001
Bus 7	LP filter only	-0.356±3.177i	0.506	0.111	-0.148±2.680i	0.426	0.055
	LP filter + 15° lag	-0.760±3.179i	0.506	0.233	-0.300±2.619i	0.417	0.114
	LP filter + 30° lag	-1.226±3.576i	0.569	0.324	-0.465±2.578i	0.410	0.178
	LP filter + 45° lag	-1.460±4.063i	0.647	0.338	-0.560±2.537i	0.404	0.215
	LP filter + 15° lead	-0.127±3.287i	0.523	0.039	-0.029±2.766i	0.440	0.010
	LP filter + 30° lead	0.012±3.428i	0.546	-0.004	0.056±2.875i	0.458	-0.020
	LP filter + 45° lead	0.065±3.542i	0.564	-0.018	0.089±2.965i	0.472	-0.030
Bus 8	LP filter only	0.021±3.883i	0.618	-0.006	-0.029±3.158i	0.503	0.009
	LP filter + 15° lag	0.049±3.892i	0.619	-0.013	-0.036±3.160i	0.503	0.011
	LP filter + 30° lag	0.092±3.906i	0.622	-0.024	-0.045±3.162i	0.503	0.014
	LP filter + 45° lag	0.141±3.931i	0.626	-0.036	-0.054±3.162i	0.503	0.017
	LP filter + 15° lead	-0.002±3.872i	0.616	0.4e-3	-0.023±3.156i	0.502	0.007
	LP filter + 30° lead	-0.022±3.857i	0.614	0.006	-0.017±3.156i	0.502	0.005
	LP filter + 45° lead	-0.032±3.840i	0.611	0.008	-0.012±3.156i	0.502	0.004
Bus 9	LP filter only	0.223±4.320i	0.688	-0.052	0.106±3.612i	0.575	-0.029
	LP filter + 15° lag	0.357±4.366i	0.695	-0.082	0.213±3.678i	0.585	-0.058
	LP filter + 30° lag	0.539±4.438i	0.706	-0.120	0.360±3.773i	0.600	-0.095
	LP filter + 45° lag	0.724±4.550i	0.724	-0.157	0.506±3.899i	0.620	-0.129
	LP filter + 15° lead	0.105±4.272i	0.680	-0.025	0.015±3.546i	0.564	-0.004
	LP filter + 30° lead	-0.014±4.196i	0.668	0.003	-0.066±3.458i	0.550	0.019
	LP filter + 45° lead	-0.089±4.104i	0.653	0.022	-0.104±3.372i	0.537	0.031

[a] This is a Reduced Two-area Power System model of Fig. 3, with only two generators, the SVC consists of a Low Pass Filter, a Lead or Lag Filter, and an Static Device #1 End Block [31], K_D =0.5, P_{78} =165 MW.

[b] This is a Full Two-area Power System model of Fig. 3, exciters are included, the SVC consists of a Low Pass Filter, a Lead or Lag Filter, and an Static Device #1 End Block [31], K_D =0.0, P_{78} =330 MW.

Results were calculated using the Multi-Area Small Signal Stability Program (MASS) from EPRI.

CHAPTER FIVE: WSCC POWER SYSTEM APPLICATION

5.1 THE CENTRAL CONTROL UNIT: MONITORING AND CONTROL - ONLINE RULES

Here, measured data from the WSCC Power System will be used in order to illustrate the online rules. Signals from BCH-Boundary, BCH-Custer, Malin-Round Mountain, Grand Coulee, and Tacoma were selected from a set of measurements provided from Bonneville Power Administration [36]. These measurements were taken during the events previous to the August 10, 1996 blackout. According with the above offline rules two subgroups were created in order to monitor the California-Oregon Interarea mode. The online rules will be described, for the time window shown in Figure 5.1 after Keeler-Allston line opens.

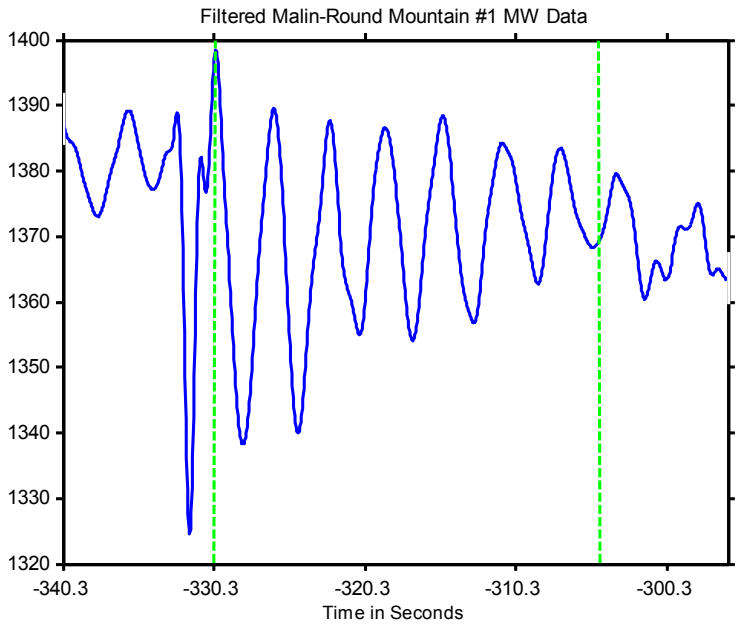

Figure 5.1: First oscillatory stage. Case 1.

5.1.1 Activation Deactivation Criteria

Multi-Prony monitoring will be triggered only after a small or medium disturbance has been detected. If not triggers are issued and no any other disturbance has occurred, the monitoring will be cancelled after 7-14 swings. Also, if triggers has been issued and based on the monitoring damping ratios are going wrong, the controller will be deactivated.

5.1.2 Validating Criteria

Crosschecking results from the same time window and for consecutive time intervals will increase reliability in the online estimations. Therefore, two criteria are developed in order to validate the Prony estimations:

1. A Prony damping estimate is considered valid only if the net variation of the damping estimates from the different subgroups is less than a threshold, say α_1. Then, the average damping estimate for the current time-window is defined as the average of the estimates from the subgroups.
2. When we consider the estimates from a consecutive set of moving time-windows, the damping estimates are used for control purposes: a) if each of the damping estimates in the different time windows is valid (i.e. they all obey the α_1 rule), and b) if the net variation of the average damping estimate from the different time windows is less than a predefined threshold say α_2.

These rules are explained through Table 5.1. Here α_1 has been set to 2%. As shown, only window five is out of the threshold and is considered not valid. This can be understood because Keeler-Allston line opening is an small disturbance and Prony's method is very accurate when there are not strong nonlinearities presented in the signals.

On the other hand, for control purposes consider the estimates of two consecutive time windows and α_2 set at 1.5%. It may be seen in Table V that the difference between the average damping ratio estimates of window 1 (5.3%) and window 2 (4.95%) are within the accepted margin difference of less than 1.5% (5.3% - 4.95% = 0.35%). However, this difference is out of the threshold for windows 2 and 3 (4.95% - 1.35% = 3.6%) and windows 3 and 4. Window 5 is not a valid estimate and windows 6 and 7 agree within the threshold.

Table 5.1: Multi-Prony COI Mode Damping
Estimation in Percent
Case 1 [a]

Time Window in Seconds [b]	P_{mr1}, P_{bound} and f_{tacoma}	P_{custer}, V_{malin} and P_{coulee}	Average	Validity
-330.3 to -318.3	5.0	5.6	5.3	Yes
-328.3 to -316.3	4.5	5.4	4.95	Yes
-326.3 to -314.3	0.4	2.3	1.35	Yes
-324.3 to -312.3	-0.4	0.0	-0.2	Yes
-322.3 to -310.3	0.3	5.0	2.65	No
-320.3 to -308.3	1.6	1.0	1.3	Yes
-318.3 to -306.3	3.0	2.3	2.65	Yes

[a] Measured data taken just after Keeler-Allston line trips at -332.3 seconds.
[b] Time with respect to Ross-Lexington line trip.
Sampling frequency is 20 samples/sec. Prony estimation was calculated using the Ringdown GUI program from BPA/PNNL Dynamic System Identification (DSI) Toolbox. Signal mean values were removed. A smoothing filter with 1 Hz cutoff frequency was used.

If a cut off damping value of 2% is used for issuing the triggers, then Table 5.1 shows that triggers would be issued at -306.3 sec using $\alpha_1 = 2\%$ and $\alpha_2 = 1.5\%$. Even though the Prony estimates in the time windows -326.3 to -314.3 and -324.3 to -312.3 are both valid, the damping estimates from these two are outside the α_2 rule. Their variation $\left(1.35\% - (-0.2\%)\right) = 1.55\% > \alpha_2 = 1.5\%$. Therefore, the triggers will not be issued at -312.3 sec. However, for the last two windows in Table 5.1, the damping estimates are valid, they are within the α_2 rule (since 2.65% - 1.3% = 1.35 < α_2), and since their

average $\frac{2.65\% + 1.3\%}{2} = 1.98\% < 2\%$, triggers will be issued at -306.3 sec for a cut off damping of 2%.

5.1.3 Selecting the SVC

An SVC priority list corresponding to each interarea mode may be built using the criteria explained in Section 4.2 for the SVC local units. These criteria may be written as:

- An SVC at the sending interarea active power flow area has more steering power than one located at the receiving area.
- Between SVC's at the same areas, the greater the corresponding SVC's *b*-*a* absolute value difference the greater the steering power.

These criteria were demonstrated in Section 4.2, and will be tested in the next WSCC power system example.

Finally, the central unit will make sure that the selected SVC will be available and working under the expected conditions by checking the actual mode content in the signals coming from the SVC location.

5.1.4 Determining the Phase Compensation

Additional to the trigger, the Central Unit will determine the type of phase compensation to be applied for the SVC with respect to the direction of the corresponding major interarea power flow. This rule was demonstrated in Section 4.2 and may be expressed as:

- An SVC in full PSDC is designed as a phase lag compensator if the SVC is at the sending side for the active power-flow of the major intertie line that is being used as the control input.

– An SVC in full PSDC is designed as a phase lead compensator if the SVC is at the receiving side for the active power-flow of the major intertie line that is being used as the control input.

5.2 THE AUGUST 10, 1996 WSCC POWER SYSTEM EXAMPLE

Measured data taken at BPA Dittmer Control Center during the events previous to the August 10, 1996 WSCC Power System breakup [36] is analyzed here in order to illustrated our approach. Also, a validated model [21] of this phenomenon is used to simulate our control strategy. Figure 5.2 shows observed data and simulated data of active power flow oscillations in one of the Malin – Round Mountain 500 kV lines, instants previous to the system breakup. From this figure, we may conclude that actual power system and the simulated model has very close dynamic behavior for the August, 10 blackout.

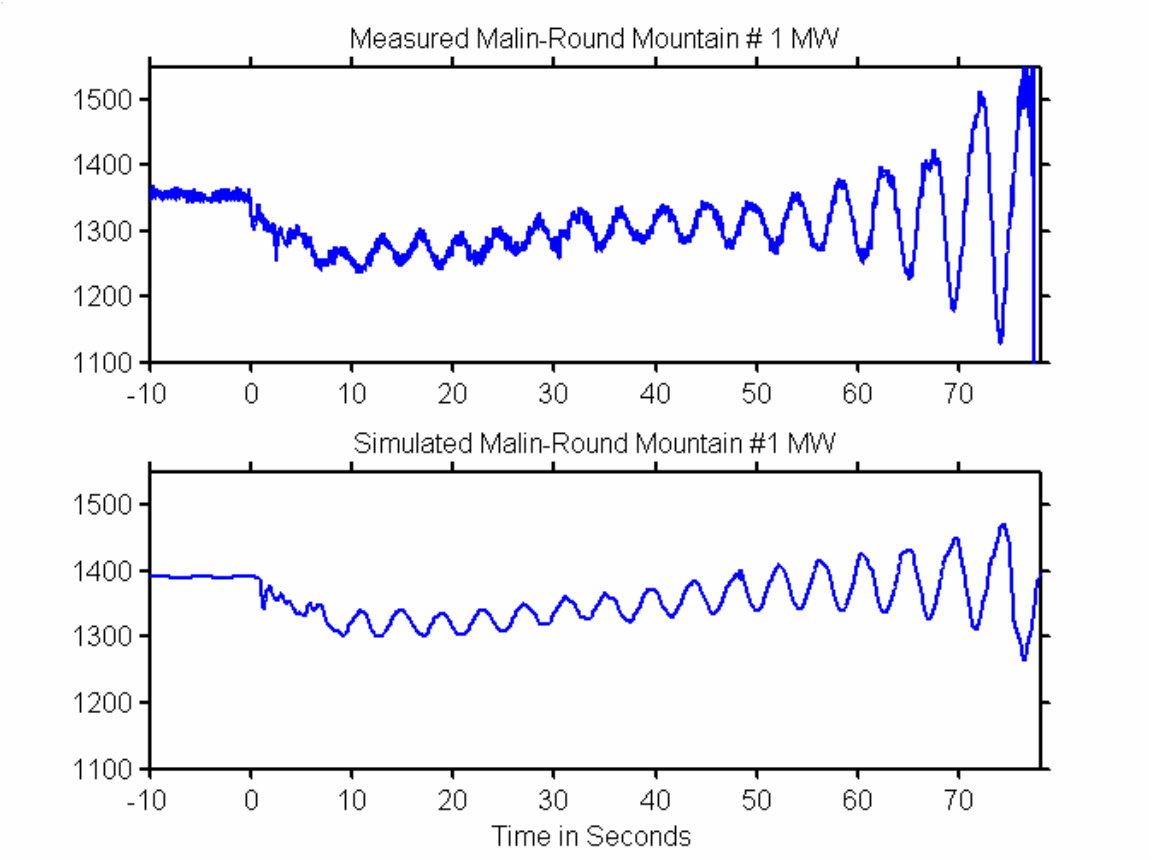

Figure 5.2: Observed and simulated growing oscillations previous to the August 10, 1996 breakup.

From Figure 1.1 and [21], two different oscillatory stages may be identified. The first oscillatory stage initiates when Keeler – Allston line trips. Ten seconds later, the Multi-Prony analysis on recorded signals shows a COI mode with a damping ratio around 1%. After this disturbance, measure data is analyzed using the Multi-Prony approach presented in this paper. The whole analyzed time window is presented in Figure 5.1.

The improved accuracy on the estimations of using Multi-Prony by groups over the single Prony, may be seen in Table 5.2 and

Table 5.3 with real data. Estimations in Table 5.2 give a wide range of possible values for the COI mode damping ratio for that time window. As seen, the estimated damping ratio values have differences of more than 4 percent.

Table 5.3 shows how grouping measurements, according to the rules developed in Section 4.1, makes the estimated damping ratio differences less than 2 percent, for the same time window.

Table 5.2: Prony Mode Parameter Estimation
WSCC Power System
(Measured Signals with COI Dominant Mode)

Symbol	Measured Signals [a]	A_i	f_i	ζ_i	Ar_i
		COI Mode			
P_{mr1}	Malin – Round Mountain #1	21.57	0.259	0.0452	1.000
P_{custer}	BCH Custer	23.08	0.263	0.0125	1.000
P_{bound}	BCH Boundary	8.372	0.259	0.0103	1.000
P_{coulee}	Grand Coulee Generation	4.041	0.244	-0.0152	1.000
V_{malin}	Malin Bus Voltage Magnitude	1.785	0.259	0.0019	1.000
f_{tacoma}	Tacoma Bus Frequency	0.006	0.233	-0.0028	0.885

[a] Time window is from -320.3 to -308.3 seconds, Figure 5.1. Ten seconds, after Keeler-Allston line trips. Sampling frequency is 20 samples/sec.

Prony estimation was calculated using the Ringdown GUI program from BPA/PNNL Dynamic System Identification (DSI) Toolbox.

Signal mean values were removed. A smoothing filter with 1 Hz cutoff frequency was used.

Table 5.3: Multi-Prony Mode Parameter Estimation
WSCC Power System
Measured Signals By Groups

Symbol		A_i	f_i	ζ_i	Ar_i
		COI Mode			
P_{mr1},		16.62			1.000
P_{bound},		8.708	0.254	0.0158	0.601
and f_{tacoma}		0.006			0.830
P_{custer}, V_{malin}, and P_{coulee}	(SVD)	(No Good Estimations)			
P_{custer}, V_{malin}, and P_{coulee}	(QR Factorization)	(No Good Estimations)			
P_{custer},		24.75			1.000
V_{malin},	(TLS)	1.889	0.256	0.0097	1.000
and P_{coulee}		4.548			0.533

Same signal measurements and programs as Table 5.2

The applied Multi-Prony analysis for the first stage is presented in Table 5.1. It shows that after the time window from -326.3 to -314.3 the estimated damping ratio is around 1 or 2 percent. If this control strategy had been implemented at that time and according to our online rules and the historical damping ratio behavior of COI mode, less than 2% cut off damping ratio would issue triggers to an SVC at Maple Valley or an SVC at Adelanto to switching from voltage regulation form to full PSDC, the August 10, 1996 blackout may have never happen, according to the simulations shown in Figure 5.3. Notice that, according with the analysis developed in section 4.2., since an SVC located at Maple Valley at that time would be at the active power sending side, the COI active power phase compensation should be lagging. On the other hand, an SVC located in Adelanto would be at the receiving active power side, the COI active power phase compensation should be leading at that bus.

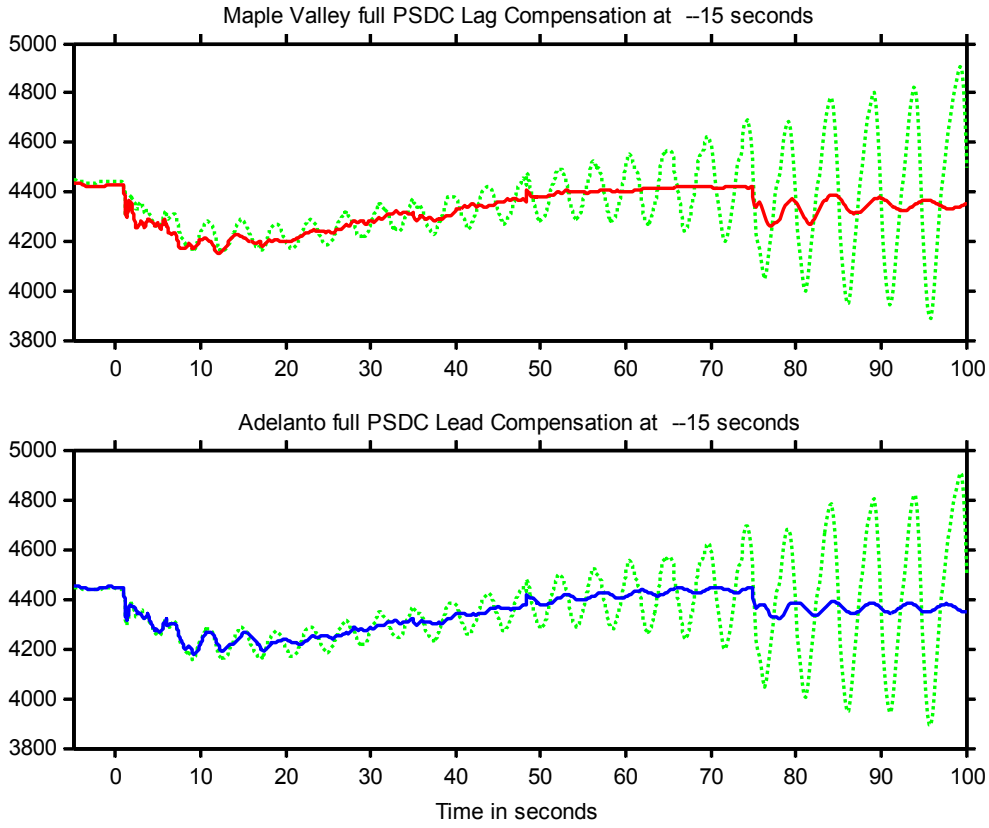

Figure 5.3: Simulated COI behavior for an SVC triggered at -15 seconds to full PSDC.

At Maple Valley with COI phase lag compensation, or at Adelanto with COI phase lead compensation.

If due to historical or technical reasons, the full PSDC compensation is not activated during the first oscillatory stage, the second stage which starts at time zero in our plots after Ross – Lexington line trips (Figure 1.1) presents a worse oscillatory scenario. At that time a sequential tripping of generators and governor actions began, introducing a stronger oscillatory behavior and also stronger nonlinearities in the signals. A closer look of this stage is presented in Figure 5.4.

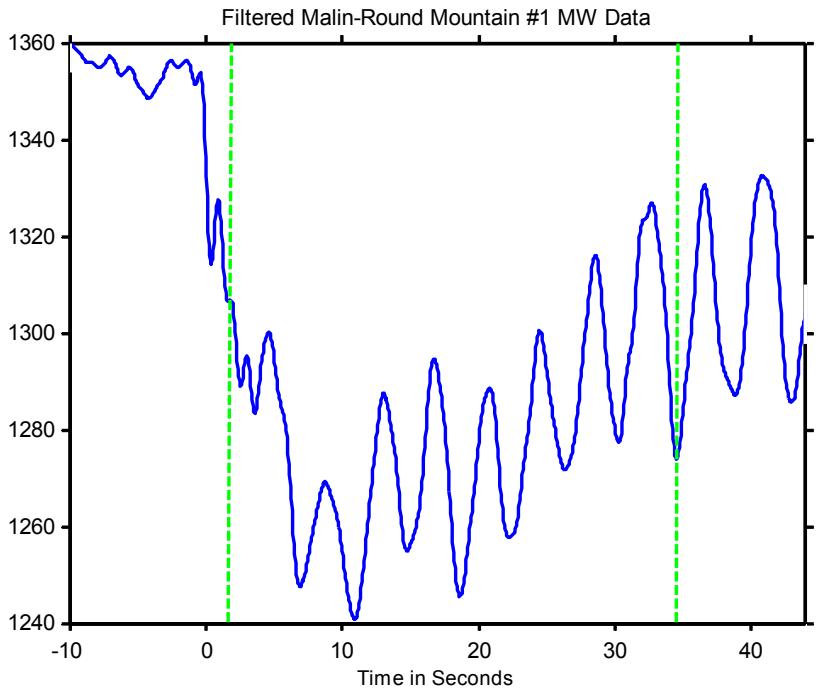

Figure 5.4: Second oscillatory stage. Case 2.

Using the same measurements from BPA, we tried to estimate the damping of these oscillations applying our multi-Prony approach by groups through the time frame defined by the dashed lines in Figure 5.4. Results are presented Table 5.4.

Table 5.4: : Multi-Prony COI Mode Damping Estimation in Percent

Case 2 [a]

Time Window in Seconds [b]	P_{mr1}, P_{bound} and f_{tacoma}	P_{custer}, V_{malin} and P_{coulee}	Average	Validity
2.0 to 14.0	-2.7	3.6	0.45	No
4.0 to 16.0	-1.3	-3.6	-2.45	No
6.0 to 18.0	1.0	1.1	1.0	Yes
8.0 to 20.0	-0.9	0.2	-0.35	Yes
10.0 to 22.0	0.0	0.8	0.4	Yes
12.0 to 24.0	1.2	1.6	1.4	Yes
14.0 to 26.0	3.5	1.9	2.7	Yes
16.0 to 28.0	1.1	0.8	0.95	Yes
18.0 to 30.0	-1.3	2.2	0.45	No
20.0 to 32.0	-2.1	-3.4	-2.75	Yes
22.0 to 34.0	-3.4	-3.1	-3.25	Yes

[a] Measured data taken just after Ross-Lexington line trips at 0.0 seconds.

[b] Time with respect to Ross-Lexington line trip.

Sampling frequency is 20 samples/sec. Prony estimation was calculated using the Ringdown GUI program from BPA/PNNL Dynamic System Identification (DSI) Toolbox. Signal mean values were removed. A smoothing filter with 1 Hz cutoff frequency was used.

Due to the strong non linearities and with an α_1 equal to 2%, the first two time windows estimations are inaccurate and they are neglected. Later, our results show that the COI mode is going lightly damped less than 1 percent damping ratio. If for control purposes we consider the estimates of 2 consecutive moving-time windows, α_2 equal to 1.5%, and a cut off value of 1% damping ratio, the central controller will issue triggers to the assigned SVC after 20 seconds. If we use 3 consecutive windows and α_2 equal to 1.5%, then the triggers would be issued at 22 sec for the same cut off damping of 1%.

However, if we want to be very conservative and wait for the mode going really unstable we may set the cut-off value at say -2% damping ratio. Then, in Table 5.4 considering only two consecutive time windows the PSDC is triggered at 34 seconds. Figure 5.5 represents the simulated behavior for this case, provide the right phase

compensation, as described in section 4.2. for an SVC located at Maple Valley, the active power sending area, and for an SVC located at Adelanto, the active power receiving area.

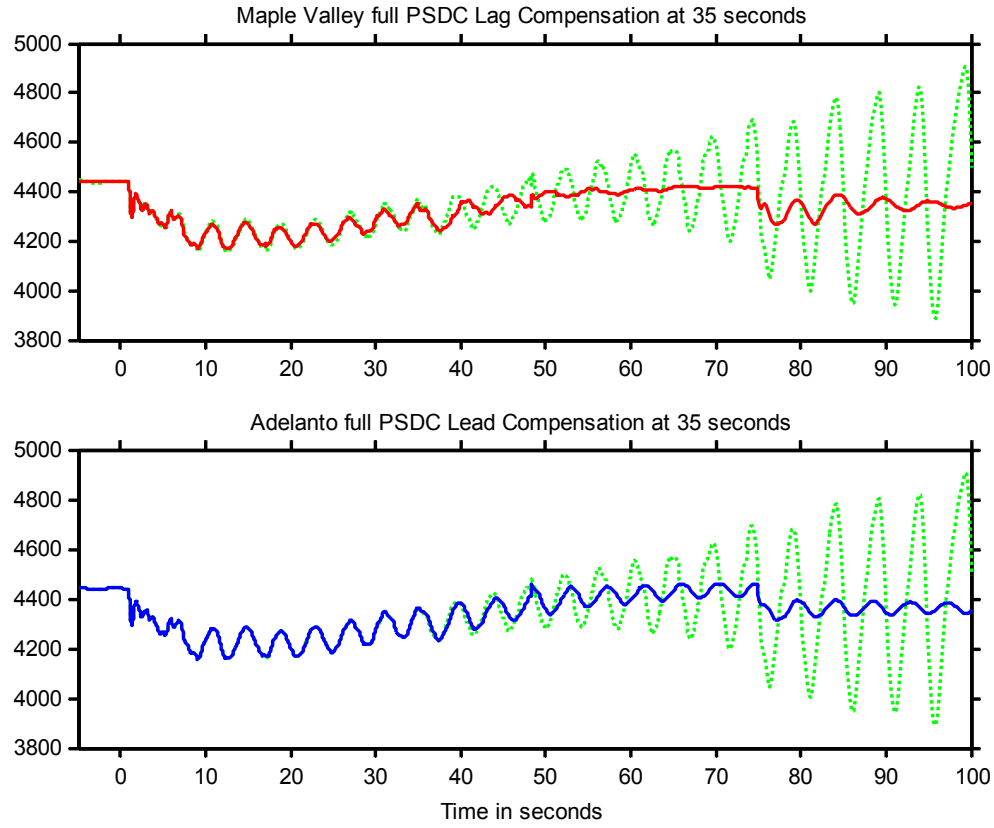

Figure 5.5: Simulated COI behavior for an SVC triggered at -15 seconds to full PSDC.

At Maple Valley with COI phase lag compensation, or at Adelanto with COI phase lead compensation.

Finally, Table 5.5 presents the frequency and damping ratios estimated from a time window from 85 to 97 seconds for the cases explained above, when the right compensation control actions are taken and when the wrong compensation control actions are applied. Notice that, as we demonstrated in section 4.2., an SVC at the sending side

has more steering power than one at the receiving side, so it could add more damping but also could be more destabilizing when right phase compensation is not applied.

Table 5.5: WSCC Power System
Simulated COI Mode Results [a]

PSDC [b] Action at	Phase Compensation	Trigged After	f	ζ
No PSDC Action			0.210	-0.0144
Mapple Valley (Sending Bus)	45° lag	Keeler-Allston trips [c]	0.181	0.0697
		Ross-Lexington trips [d]	0.183	0.0908
	60° lead	Keeler-Allston trips [c]	System Collapses	
		Ross-Lexington trips [d]	System Collapses	
Adelanto (Receiving Bus)	45° lag	Keeler-Allston trips [c]	0.240	-0.0216
		Ross-Lexington trips [d]	0.220	-0.0289
	60° lead	Keeler-Allston trips [c]	0.229	0.0284
		Ross-Lexington trips [d]	0.230	0.0201

[a] Time window is from 85 to 97 seconds.
[b] SVCs are originally working in Bus Voltage Regulation Control.
[c] Full PSDC function trigs at -15 seconds.
[d] Full PSDC function trigs at 35 seconds

On the other hand, it may be of interest the behavior of the SVC Bus voltage magnitude and the SVC output during the full PSDC operation. These variables are presented in the following figures, when the SVC is triggered at -15 seconds. Notice that when the appropriate phase compensation is applied, Figure 5.6 and Figure 5.8, voltage regulation in full PSDC mode is worse than in voltage regulation mode during the first seconds. However, after unstable interarea oscillations become large for the voltage regulation mode, voltage signals become also unstable.

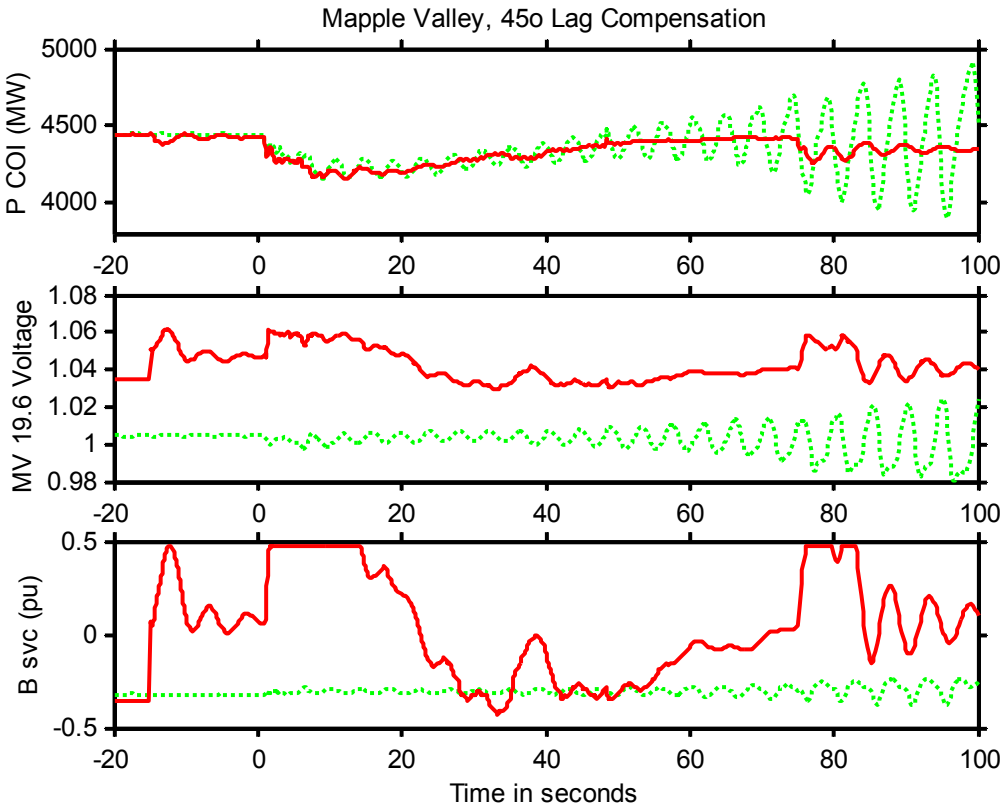

Figure 5.6: Simulated WSCC Power System behavior for an SVC triggered to full PSDC at -15 seconds.

Dotted line: SVC in VR mode. Solid line: SVC in PSDC mode

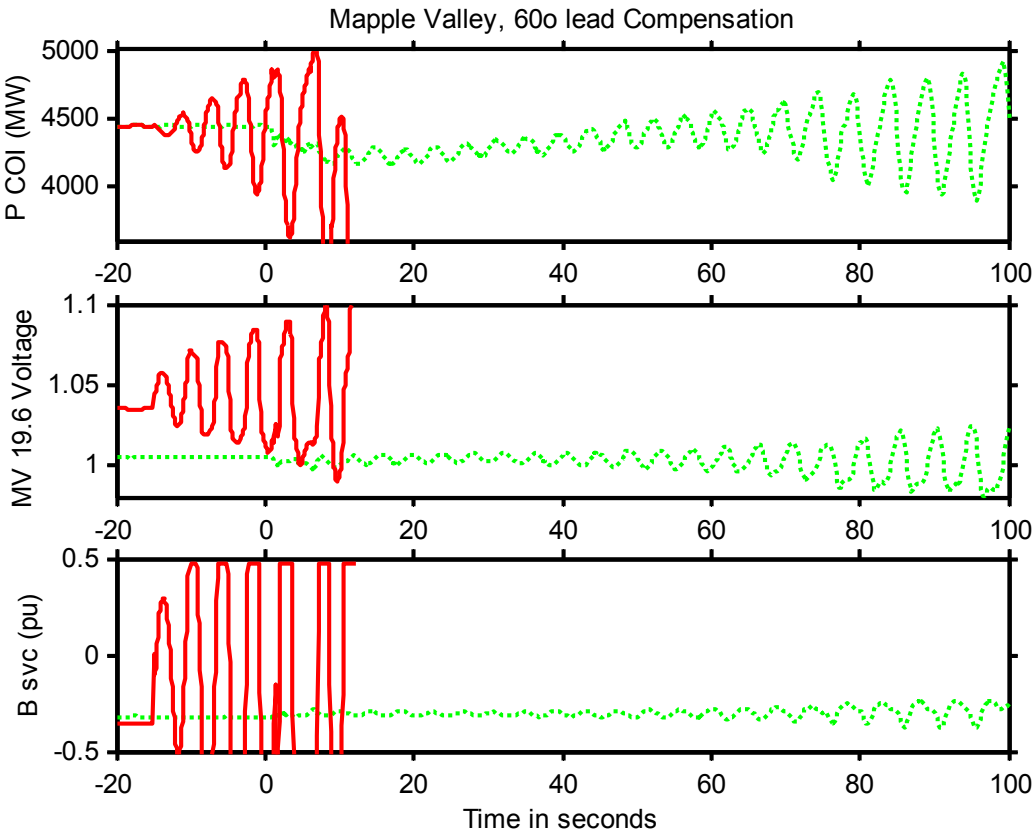

Figure 5.7: Simulated WSCC Power System behavior for an SVC triggered to full PSDC at -15 seconds.

Dotted line: SVC in VR mode. Solid line: SVC in PSDC mode

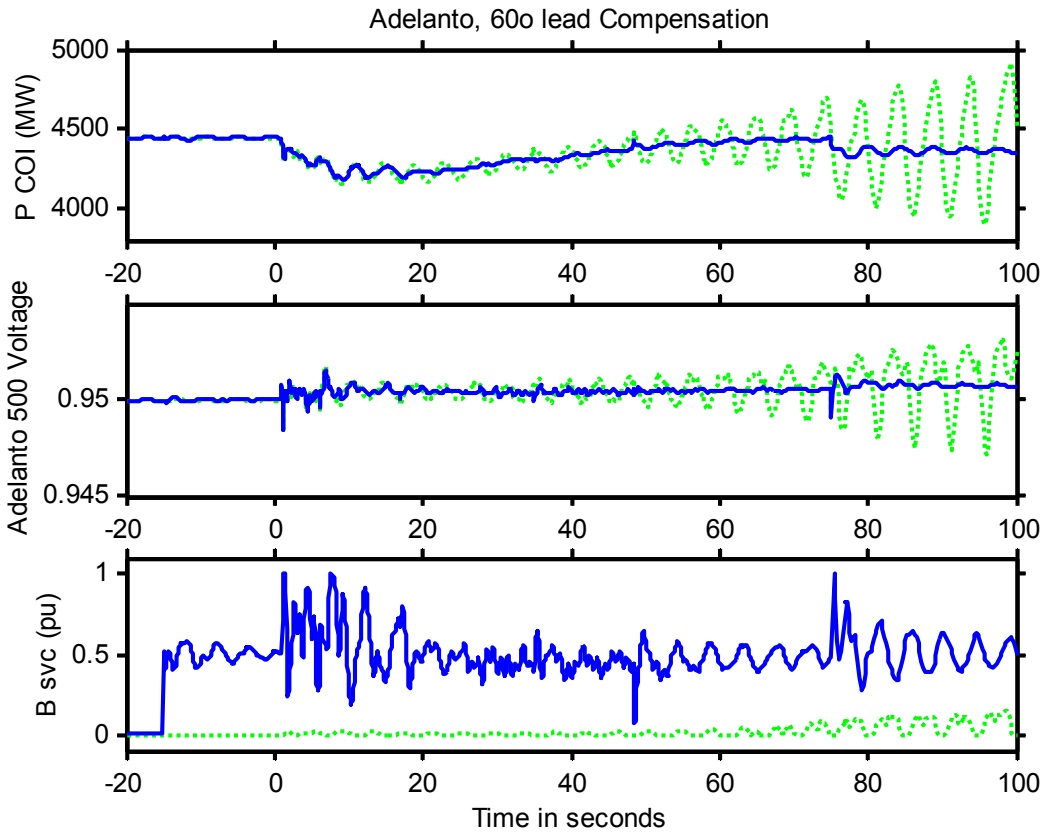

Figure 5.8: Simulated WSCC Power System behavior for an SVC triggered to full PSDC at -15 seconds.

Dotted line: SVC in VR mode. Solid line: SVC in PSDC mode

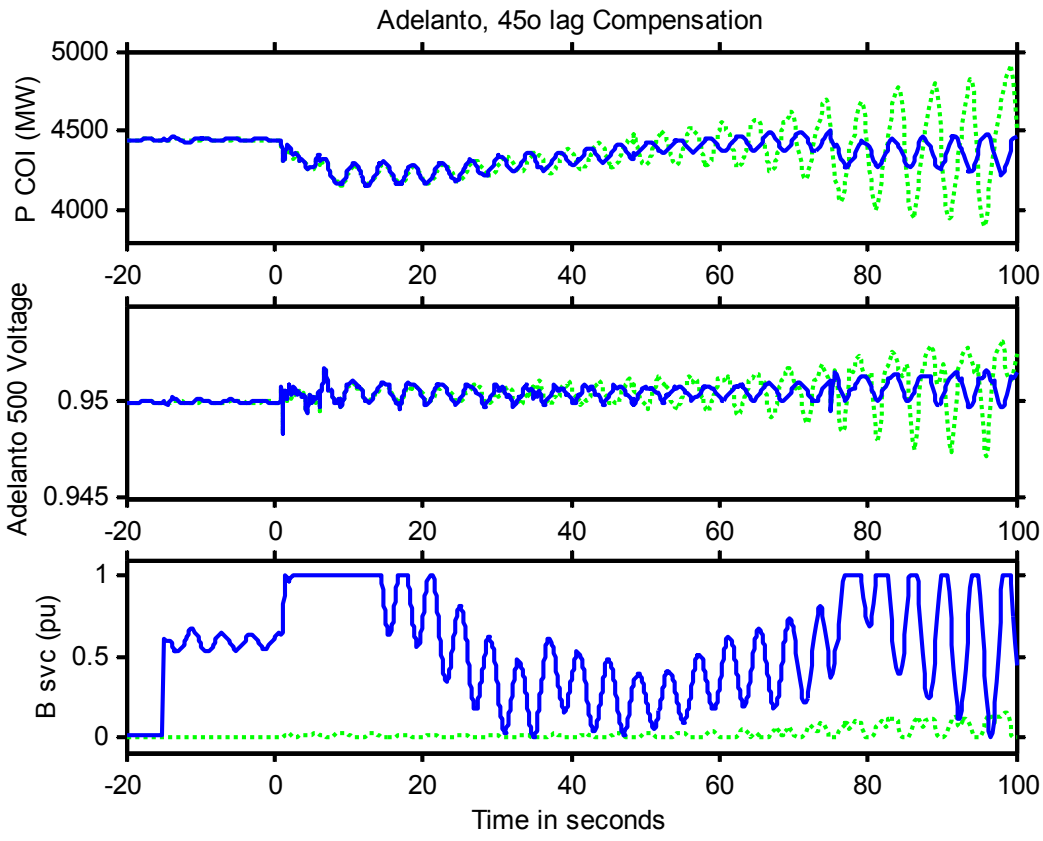

Figure 5.9: Simulated WSCC Power System behavior for an SVC triggered to full PSDC at -15 seconds.

Dotted line: SVC in VR mode. Solid line: SVC in PSDC mode

CHAPTER SIX: CONCLUSIONS

This paper presents a powerful and practical real-time wide-area controller which is specifically aimed at improving the dynamic security in the small-signal sense. This real-time control strategy showed how with increased observability and reliability, the Multi-Prony analysis can be successfully applied on real-time basis for detecting the proximity and onset of small-signal instability phenomena, while avoiding the pitfalls and the shortcomings widely known and reviewed in the Prony literature. The controller then initiates aggressive mitigatory control actions in certain areas by using commonly available resources such as the SVC's in modern power networks. The controller will come into play only under extremely stressed operating conditions when the damping of some oscillatory modes becomes problematic.

Recent black-out events such as the 1996 western American events, 2004 Noreastern disturbance and the 2004 Italian black-out have clearly demonstrated that the power system will repeatedly find itself in highly stressed unplanned for operating scenarios. We need to design new automatic controllers which are specifically targeted towards such unforeseen operating conditions which mitigate the problem from cascading into big black-outs. This paper proposes one such "safety net" controller for stabilizing the large system while facing small-signal instability problems.

Including HVDC links and other FACTS devices should be part of a future work. Also, analyzing an optimal signal mode identification method for power system measurements would be of interest. Other approaches for handling transient stability problems in real-time in the large system promise to be more challenging for future research.

REFERENCES

[1] C. Taylor, D. Erickson, B. Wilson, and K. Martin. (2002, December 16). Wide-Area Stability and Voltage Control System (WACS) Demostration (Living Document). Available: http://www.transmission.bpa.gov/orgs/opi/index.shtm

[2] K. Tomsovic, D. Bakken, V. Venkatasubramanian, A. Bose, "Designing the Next Generation of Real-Time Control, Communication and Computations for Large Power Systems," *IEEE Proc. – Special Issue on Energy Infrastructure Systems,* submitted for publication.

[3] U.S.–Canada Power System Outage Task Force, "Causes of the August 14th Blackout in the United States and Canada," Interim Rep., Nov. 2003, ch. 6.

[4] A. E. Hammad, "Analysis of power system stability enhancement by static var compensators," *IEEE Trans. Power Systems*, vol. PWRS-1, pp. 222-227, Nov. 1986.

[5] E. Lerch, D. Povh, and L. Xu, "Advanced SVC control for damping power system oscillations," *IEEE Trans. Power Systems*, vol. 6, pp. 524-535, May 1991.

[6] R. L. Lee, M. J. Beshir, A. T. Finley, D. R. Hayes, J. C. Hsu, H. R. Peterson, G. L. DeShazo, and D. W. Gerlach, "Application of static var compensators for the dynamic performance of the Mead-Adelanto and Mead-Phoenix transmission projects," *IEEE Trans. Power Delivery*, vol. 10, pp. 459-466, Jan. 1995.

[7] J. R. Smith, D. A. Pierre, D. A. Rudberg, I. Sadighi, A. P. Johnson, and J. F. Hauer, "An enhanced LQ adaptive var unit controller for power system damping," *IEEE Trans. Power Systems*, vol. 4, pp. 443-451, May 1989.

[8] K. M. Son and J. K. Park, "On the robust LQG control of TCSC for damping power system oscillations," *IEEE Trans. Power Systems*, vol. 15, pp. 1306-1312, Nov. 2000.

[9] Q. Zhao and J. Jiang, "Robust SVC controller design for improving power system damping," *IEEE Trans. Power Systems*, vol. 10, pp. 1927-1932, Nov. 1995.

[10] X. Yu, M. Khammash, and V. Vittal, "Robust design of a damping controller for static var compensators in power systems," *IEEE Trans. Power Systems*, vol. 16, pp. 456-462, Aug. 2001.

[11] H. Bourlès, S. Peres, T. Margotin, and M. P. Houry, "Analysis and design of a robust coordinated AVR/PSS," *IEEE Trans. Power Systems*, vol. 13, pp. 568-575, May 1998.

[12] I. Kamwa, G. Trudel, and L. Gérin-Lajoie, "Robust design and coordination of multiple damping controllers using nonlinear constrained optimization," *IEEE Trans. Power Systems*, vol. 15, pp. 1084-1092, Aug. 2000.

[13] J. C. R. Ferraz, N. Martins, and G. N. Taranto, "Simultaneous partial pole placement for power system oscillation damping control," presented at the IEEE Winter Power Meeting, 28 Jan. - 1 Feb., 2001, pp. 1154-1159.

[14] J. J. Sanchez-Gasca, "Coordinated control of two FACTS devices for damping interarea oscillations," *IEEE Trans. Power Systems*, vol. 13, pp. 428-434, May 1998.

[15] P. Pourbeik and M. J. Gibbard, "Simultaneous coordination of power system stabilizers and FACTS device stabilizers in a multimachine power system for enhancing dynamic performance," *IEEE Trans. Power Systems*, vol. 13, pp. 473-479, May 1998.

[16] X. Lei, E. N. Lerch, and D. Povh, "Optimization and coordination of damping controls for improving system dynamic performance," *IEEE Trans. Power Systems*, vol. 16, pp. 473-480, Aug. 2001.

[17] I. Kamwa, R. Grondin, and Y. Hébert, "Wide-area measurement based stabilizing control of large power systems – A decentralized/hierarchical approach," *IEEE Trans. Power Systems*, vol. 16, pp. 136-153, Feb. 2001.

[18] G. E. Boukarim, S. Wang, J. H. Chow, G. N. Taranto, and N. Martins, "A comparison of classical, robust, and decentralized control designs for multiple power system stabilizers," *IEEE Trans. Power Systems*, vol. 15, pp. 1287-1292, Nov. 2000.

[19] M. J. Gibbard, N. Martins, J. J. Sanchez-Gasca, N. Uchida, V. Vittal, and L. Wang, "Recent applications of linear analysis techniques," *IEEE Trans. Power Systems*, vol. 16, pp. 154-162, Feb. 2001.

[20] M. Klein, G. J. Rogers, and P. Kundur, "A Fundamental Study of Inter-Area Oscillations in Power Systems," *IEEE Trans. Power Systems,* vol. 6, pp. 914-921, Aug. 1991.

[21] D. N. Kosterev, C. W. Taylor, and W. A. Mittelstadt, "Model validation for the August 10, 1996 WSCC system outage," *IEEE Trans. Power Systems*, vol. 14, pp. 967-979, Aug. 1999.

[22] G. R. B. Prony, "Essai experimental et analytique sur les lois de la dilatalrlite de fluids elastiques et sur cells de la vapeur de l'alcool, à différents tempoeratures," Journal de *l'Ecole Polytechnique (París),* vol. 1, pp. 24-76, 1795.

[23] D. J. Trudnowski, J. R. Smith, T. A. Short, and D. A. Pierre, "An application of Prony methods in PSS design for multi-machine systems," *IEEE Trans. Power Systems*, vol. 6, pp. 118-126, Feb. 1991.

[24] P. S. Dolan, J. R. Smith, and W. A. Mittelstadt, "Prony analysis and modeling of a TCSC under modulation control," in *Proc. 4th IEEE Conference on Control Applications*, 1995, Sept. 1995, pp. 239 – 245.

[25] M. Amono, M. Watanabe, M. Banjo, "Self-testing and self-tuning of power system stabilizers using Prony analysis," in *Proc. IEEE Winter Power Meeting,* 1999, pp. 655-660.

[26] S. W. Chen, "A two-stage discrimination of cardiac arrhythmias using a total least squares-based Prony modeling algorithm," *IEEE Trans. Biomedical Engineering,* vol. 47, pp. 1317-1327, Oct. 2000.

[27] F. M. El-Hefnawi, "Use of Prony's method for extracting the poles and zeros yielding a wideband window type response of circular antenna arrays," in *Proc. IEEE Radio and Wireless Conference*, 1998, pp. 201-204.

[28] K. F. Sabett, L. P. B. Katehi, and K. Sarabandi, "Wavelet-based CAD modeling of microstrip discontinuities using least square Prony's method," in *Proc. IEEE MTT-S International,* 1997, pp. 1799-1802.

[29] M. Meunier, F. Brouaye, "Fourier transform, wavelets, Prony analysis: tools for harmonics and quality of power," in *Proc. 8th International Conf. Harmonics and Quality of Power,* 1998, pp. 71-76.

[30] M. A. Andrade, A. R. Messina, C. A. Rivera, and D. Olguin, "Identification of Instantaneous Attributes of Torsional Shaft Signals using the Hilbert Transform," *IEEE Trans. Power Systems,* to be published.

[31] D. Ruiz-Vega, A. R. Messina, and M. Pavella, "Online Assessment and Control of Transient Oscillations Camping," *IEEE Trans. Power Systems,* vol. 19, pp. 1038-1047, May. 2004.

[32] J. Xiao, X. Xie, J. Han, and J. Wu, "Dynamic Tracking of Low-frequency Oscillations with Improved Prony Method in Wide-Area Measurement System," presented at the IEEE Power Meeting, Denver, CO, June 6-10, 2004.

[33] R. Zivanovic, P. Schegner, "Pre-filtering improves prony analysis of disturbance records," in *Proc. IEE Int. Conf. Developments in Power System Protection,* 2004, pp. 780-783.

[34] M. A. Johnson, I. P. Zarafonitis, M. Calligaris, "Prony analysis and power system stability-some recent theoretical and applications research," in *Proc. IEEE Power summer Meeting,* 2000, pp. 1918-1923.

[35] J. F. Hauer, C. J. Demeure, and L. L. Scharf, "Initial Results in Prony Analysis of Power System Response Signals," *IEEE Trans. Power Systems,* vol. 5, pp. 80-89, Feb. 1990.

[36] *BPA/PNNL Dynamic Systems Identification (DSI) Toolbox: Version 3.0.4*, Battelle Memorial Institute, 1998.

[37] D. J. Trudnowski, J. M. Johnson, and J. F. Hauer, "SIMO System Identification from Measured Ringdowns," in 1998 *Proc. American Control Conf.,* pp. 2968-2972.

[38] P. Kundur, *Power System Stability and Control.* McGraw-Hill, 1994.

[39] H. K. Hassan, *Nonlinear Systems,* 2nd ed. Upper Saddle River: Prentice Hall, 1996.

[40] C.-T. Chen, *Linear System Theory and Design,* 3rd ed. New York: Oxford University Press, 1999.

[41] I. J. Pérez-Arriaga, G. C. Verghese, and F. C. Schweppe, "Selective Modal Analysis with Applications to Electric Power Systems, Part I: Heuristic Introduction," *IEEE Trans. Power Apparatus and Systems,* vol. 101, pp. 3117-3125, Sep. 1982.

[42] F. B. Hildebrand, *Introduction to numerical analysis*. New York: McGraw-Hill, 1956.

[43] J. G. Proakis, C. M. Rader, F. Ling, C. L. Nikias, M. Moonen, and I. K. Proudler, *Algorithms for Statistical Signal Processing.* Upper Saddle River: Prentice Hall, 2002.

[44] P. M. Anderson and A. A. Fouad, *Power System Control and Stability.* New York: IEEE Press, 1994.

[45] *Extended Transient-Midterm Stability Program (ETMSP): Version 3.1*, Volume 2, User's manual, Electric Power Research Institute, Palo Alto, CA, 1994.

[46] K. W. Schneider, "Application of Power Swing Damping Control (PSDC) on an SVC to improve Transient Stability of the WSCC Interconnected System," M.S. thesis, Dept. Elect. Eng. Comp. Science, Washington State Univ., Pullman, USA, 1999.